Host influenced geochemical signature in the parasitic foraminifer *Hyrrokkin sarcophaga*

Nicolai Schleinkofer[1,2], David Evans[1,2], Max Wisshak[3]; Janina Vanessa Büscher[4,5], Jens Fiebig[1,2], André Freiwald[3], Sven Härter[1], Horst R. Marschall[1,2], Silke Voigt[1,2], Jacek Raddatz[1,2]

[1]Goethe Universität Frankfurt, Institut für Geowissenschaften, Frankfurt am Main, Germany

[2]Goethe Universität Frankfurt, Frankfurt Isotope and Element Research Center (FIERCE), Frankfurt am Main, Germany

[3]Senckenberg am Meer, Marine Research Department, Wilhelmshaven, Germany

[4]National University of Ireland Galway, Department of Earth and Ocean Sciences, Galway, Ireland

[5]GEOMAR Helmholtz Centre for Ocean Research Kiel, Department of Biological Oceanography, Kiel, Germany

Corresponding Author: Nicolai Schleinkofer (schleinkofer@em.uni-frankfurt.de)

Abstract

Hyrrokkin sarcophaga is a parasitic foraminifera that is commonly found in cold-water coral reefs where it infests the file clam *Acesta excavata* and the scleractinian coral *Desmophyllum pertusum* (formerly known as *Lophelia pertusa)*. Here, we present measurements of the trace-element and isotopic composition of these parasitic foraminifera, analyzed by inductively coupled optical emission spectrometry (ICP-OES), electron probe micro analysis (EPMA) and mass spectrometry (Gas-source-MS and Inductively-coupled-plasma-MS).

Our results reveal that the geochemical signature of *H. sarcophaga* depends on the host organism it infests. Sr/Ca ratios are 1.1 mmol mol^{-1} higher in *H. sarcophaga* that infest *D. pertusum*, which could be an indication that dissolved host carbonate material is utilised in shell calcification, given that the aragonite of *D. pertusum* has a naturally higher Sr concentration compared to the calcite of *A. excavata*. Similarly, we measure 3.1 ‰ lower $\delta^{13}C$ and 0.25 ‰ lower $\delta^{18}O$ values in *H. sarcophaga* that lived on *D. pertusum*, which might be caused by the direct uptake of the host's carbonate material with a more negative isotopic composition or different pH regimes in these foraminifera (pH can exert a control on the extent of CO_2 hydration/hydroxylation) due to the uptake of body fluids of the host. We also observe higher Mn/Ca ratios in foraminifera that lived on *A. excavata* but did not penetrate the host shell compared to specimen that penetrated the shell, which could be interpreted as a change in food source, changes in the calcification rate, Rayleigh fractionation or changing oxygen conditions.

While our measurements provide an interesting insight into the calcification process of this unusual foraminifera, these data also indicate that the geochemistry of this parasitic foraminifera is unlikely to be a reliable indicator of paleoenvironmental conditions using Sr/Ca, Mn/Ca, $\delta^{18}O$ or $\delta^{13}C$ unless the host organism is known and its geochemical composition can be accounted for.

1. Introduction

The foraminifera are a very diverse group of marine shelly organisms that are commonly used for paleoenvironmental reconstructions using the isotopic or elemental composition of their carbonate shell (Petersen et al., 2018; Hönisch et al., 2011; Gray and Evans, 2019; Lear and Rosenthal, 2006; Raddatz et al., 2017). They first appeared in the Cambrian and, over the course of the Phanerozoic, occupied oceanic settings from coastal waters to the open ocean, as well as deep sea benthic habitats (Goldstein, 1999). Multiple feeding methods are known from foraminifera, including suspension feeding, grazing, predation and parasitic feeding (Hancock et al., 2015). The latter is probably the least common feeding mechanism among the foraminifera with only nine species that are known to be parasitic and a further 13 that are suspected to be (Walker et al., 2017). One of the known parasitic species is *Hyrrokkin sarcophaga* (Cedhagen, 1994), a common foraminifera in cold-water coral reefs in the NE-Atlantic (Beuck et al., 2008). *H. sarcophaga* preferentially colonises the file clam *Acesta excavata*, but also other organisms such as the bivalve *Delectopecten vitreus*, sponges of the family Geodiidae and Ancorinidae, cold-water corals such as *Desmophyllum pertusum* (formerly known as *Lophelia pertusa* (Addamo et al., 2016)*), Madrepora occulata* and *Flabellum japonicum,* as well as other foraminifera (Beuck et al., 2008; Cheng and Dai, 2016; Cedhagen, 1994). Besides biogenic hard substrates, *H. sarcophaga* can also be found settling on rocks which shows that it can at least survive short periods without a host (Cedhagen, 1994). *H. sarcophaga* forms an attachment etching, i.e. mirroring its spiral outline on the host. From this depression the foraminifera etch a canal into the shell of the host (Cedhagen, 1994) (Fig. 1). This allows the foraminifera to feed on the bivalve host's tissue (Cedhagen, 1994) and possibly assimilate amino acids from its extrapallial calcifying fluid (Schweizer et al., 2012; Alexander and Delaca, 1987).

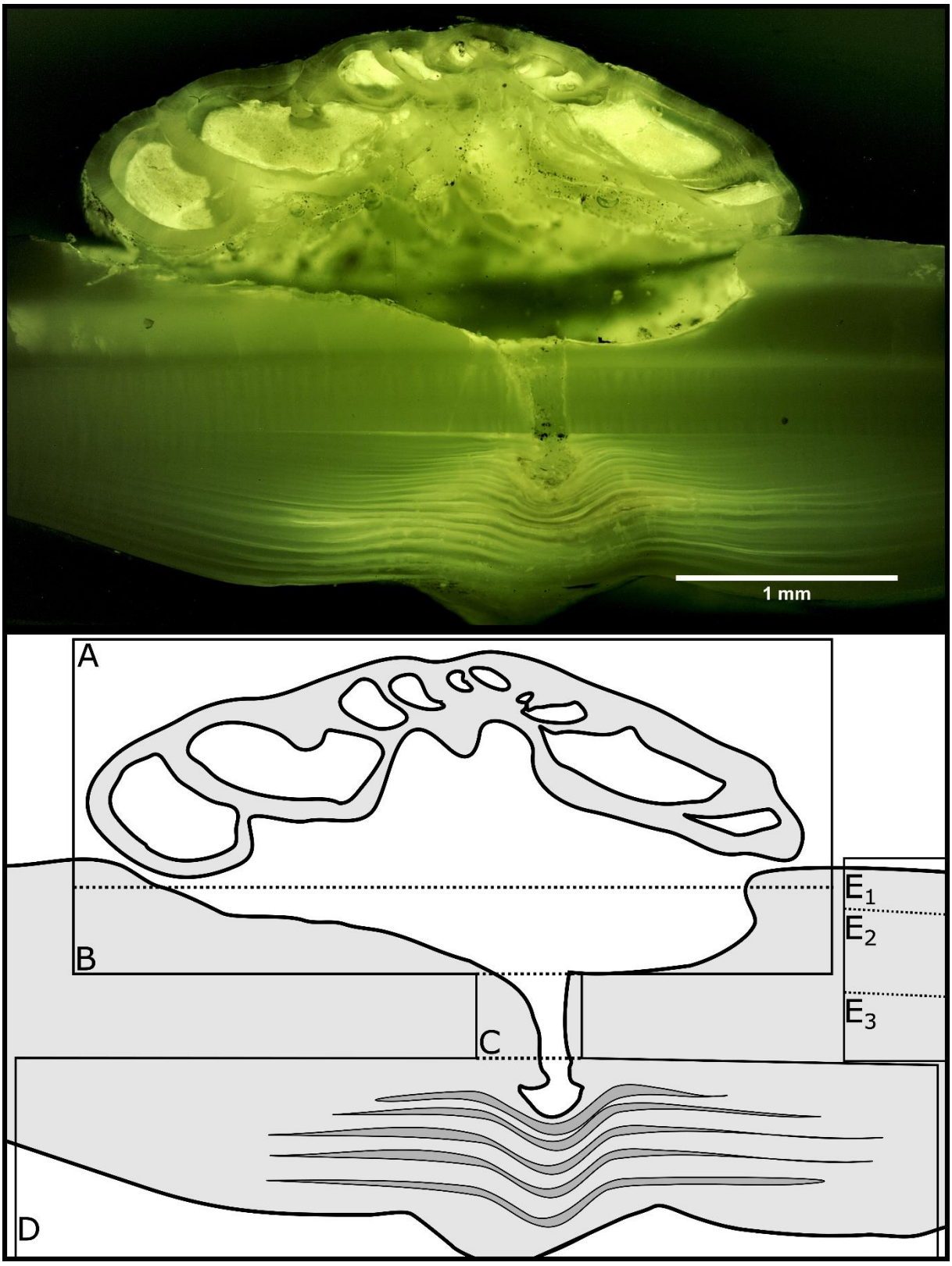

Figure 1 Fluorescence microscopic image (excitation 420 – 490 nm) and schematic figure of *H. sarcophaga* on *A. excavata*. A: *H. sarcophaga*, B: Attachment depression corroded by *H. sarcophaga*, C: Bored canal, D: Callus built by *A. excavata* (SRZ = shell repair zone), E: Undisturbed shell, E_1: Calcitic shell layer (fibrous), E_2: Calcitic shell layer (microgranular), E_3: Aragonitic shell layer

The bivalve reacts by building a callus (layered aragonite rich in organics) to seal this boring (Fig 1D) and defend the organism from the parasite's attack (Beuck et al., 2008). In *D. pertusum*, borings into the inner calyx area were not observed (Beuck et al., 2008). Instead, multiple "whip"-shaped tunnels protrude into the coral's skeleton, which possibly serve an anchoring function (Beuck et al., 2008). The pit is possibly formed either as a way to protect itself from cleaning attempts of the host and increase attachment strength or to serve the foraminifera's need for calcium and/or DIC (Beuck et al., 2008; Cedhagen, 1994).

As the parasitic foraminifera ingests material from its host, the question arises whether this process exerts an influence on the shell geochemistry of the parasite. Should this be the case, this factor may need to be accounted for, especially as some parasitic foraminifera, such as *Cibicides refulgens,* are also used in geochemical studies for paleoenvironmental reconstructions (García-Gallardo et al., 2017; Mackensen and Nam, 2014; Rathburn and de Deckker, 1997; Raddatz et al., 2011; Alexander and Delaca, 1987).

Here, we present element to Ca ratios (Mg/Ca, Sr/Ca, Na/Ca and Mn/Ca) and stable isotope data (oxygen and carbon) analyzed in *H. sarcophaga* collected from different host organisms (*A. excavata* and *D. pertusum*) from the Trondheimsfjord (Norway) to explore if and how the different hosts influence the geochemical composition of the test of foraminifera. In addition, we present element maps analyzed by electron microprobe analysis (EPMA) of the callus region of *A. excavata* in order to explore geochemical differences between the callus region and undisturbed shell areas.

2. Material and Methods

2.1. Sampling

All investigated samples were collected in the Leksa Reef, located at the entrance to the Trondheimsfjord in Norway (N 63.613056/E 9.384167, depth ~ 200 m) by means of the manned submersible JAGO (GEOMAR Helmholtz-Zentrum für Ozeanforschung, 2017) during the scientific cruises POS473 and POS525 with RV *Poseidon* (Form et al., 2015; Büscher, 2018; GEOMAR Helmholtz-Zentrum für Ozeanforschung, 2015). In total we analyzed 30 specimens of *H. sarcophaga*, which were divided into three groups: 1. *H. sarcophaga* that infested *A. excavata* with callus formation (henceforth called HAW), 2. *H. sarcophaga* that infested *A. excavata* without callus formation (henceforth called HAO; HAW + HAO = HA), 3. *H. sarcophaga* that infested *D. pertusum* (henceforth called HL). Samples of *A. excavata* and *D. pertusum* were alive when sampled. We cannot be entirely certain that *H. sarcophaga* were still alive when sampled, but upon death they easily become detached from the shell whereas in our samples the foraminifera were still firmly attached. For ICP-OES, ICP-MS and GS-MS,

the samples were ultrasonically rinsed in deionized water for five minutes and allowed to dry before crushing in an agate mortar

2.2. Shell carbonate polymorph

The polymorph of the foraminiferal shell was determined using cobalt nitrate solution (Meigen solution). The foraminifera samples were crushed in an agate mortar and transferred to Eppendorf containers. The samples were mixed with 10 wt% $Co(NO_3)_2$ aqueous solution and allowed to react at 95°C for 20 minutes. Afterwards the samples were washed four times with deionized-water and inspected under a KEYENCE VHX-S660E microscope. Aragonite stains purple/pink in cobalt nitrate solution, whereas calcite remains unaffected (Kato et al., 2003)

2.3. Fluorescence microscopy

We used fluorescence microscopy to investigate the distribution of the organic material in the foraminifera and the underlying bivalve shell. The sample was cut, ultrasonically cleaned in deionized-water, embedded in epoxy resin (Araldite 2020) and polished with 3 µm diamond-lapping paste Fluorescent images were taken using a Leica DMRX-POL microscope with fluorescent front light and a 50 W mercury lamp. The microscope was equipped with an H3 filter cube, which excites in the wavelength range of blue to violet (Bandpass filter: 420 – 490 nm) The pictures were taken with a digital camera connected to the microscope with 0.25 s exposure time.

2.4. EPMA

Two samples of *A. excavata* with attached *H. sarcophaga* were analysed by electron probe micro analysis (EPMA). The area of interest was cut from the shell with a handheld drilling tool, ultrasonically cleaned in deionized-water for five minutes, mounted vertically into circular mounts and embedded in epoxy resin (Araldite 2020). The sample surface was ground with 9 µm grid with silicon carbide sanding paper and then polished using 3 µm diamond-water based lapping paste. After polishing the samples were coated with carbon.

The EPMA analyses were conducted at Goethe University Frankfurt on a JEOL JXA-8530F Plus Field Emission Gun Electron Probe Micro Analyzer (FEG-EPMA). Analysis conditions were: 15 kV acceleration voltage, 20 nA current with a beam diameter of 3 µm. We used a TAP crystal for Mg, TAPL for Na and Sr and PETH for S. Detection limits are calculated with the equation given in Goldstein et al., 2017 and amount to: Mg = 178 µg g^{-1} (Mg/Ca = 0.7 mmol mol^{-1}), Na = 170 µg g^{-1} (Na/Ca = 0.7 mmol mol^{-1}), Sr = 129 µg g^{-1} (Sr/Ca = 0.1 mmol mol^{-1}), S = 152 µg g^{-1} (S/Ca = 0.4 mmol mol^{-1}) and Ca = 195 µg g^{-1}.Molar ratios were calculated from the weight fractions of the specific oxides (CaO, MgO, Na_2O, SrO, SO_3) by calculating the concentration of the observed elements (in µg/g) and normalization to Ca accounting

for their relative atomic mass. The chemical maps were recorded with a beam diameter of 2 µm, 15 kV acceleration voltage and 20 nA current.

2.5. ICP-OES

For ICP-OES measurements we used ten HAW, ten HAO and ten HL samples. About 120 µg of sample powder was transferred to Eppendorf tubes (acid cleaned with 5 % HNO_3) and sealed. Each sample was analyzed three times.

Elemental ratios Mg/Ca, Sr/Ca, Na/Ca and Mn/Ca (only for foraminifera and bivalves) were analyzed by inductively coupled plasma-optical emission spectrometry (ICP-OES). ICP-OES analysis was carried out using a Thermoscientific iCap 6300 Duo at the Institute of Geosciences, Goethe University Frankfurt. The sample powder (≈ 140 µg) was dissolved in 500 µL HNO_3 (2%) and 300µL aliquots were separated. Subsequently 1500 µL of 1.2 mg L^{-1} yttrium solution was added to each aliquot as an internal standard resulting in a concentration of Y= 1mg L^{-1} and Ca = 25mg L^{-1}. The intensity data were background corrected, standardized internally to Y and normalized to Ca. Accuracy is reported in %-deviation from values of standard reference material JCP1 and USGS MACS-3 (n = 5)(Jochum et al., 2005) and is better than 1% for Mg/Ca and Sr/Ca, 5% for Na/Ca and 3% for Mn/Ca. Precision is reported in relative standard deviation; % RSD of the USGS MACS-3 and JCP1 carbonate reference material (n = 5)(Jochum et al., 2005) and is better than 3% for all analyzed elements.

Bivalve (n = 3) and coral (n = 3) samples were treated similarly to foraminifera samples. We took 15 - 20 samples per shell from the outermost shell section along the main growth axis, starting at the ventral margin resulting in a total of 49 samples. The corals were sampled randomly over the whole calyx area resulting in 44 samples.

2.6. ICP-MS

The manganese concentration of *D. pertusum* had to be determined by ICP-MS because it was below the limit of detection by ICP-OES. We used three specimens (two from the Leksa Reef, one from the Sula Reef) of which we sampled 150 µg from the fibrous shell section. Each sample was measured twice.

For solution based ICP-MS measurements we used 150 µg of sample powder and dissolved it in 500 µL 2% HNO_3. The dissolved sample (300 µL) was mixed with 1500 µL 1.2 mg L^{-1} yttrium solution which was used as the internal standard. The reference material ECRM 752-1 (Greaves et al., 2008) was used to monitor measurement precision and accuracy, reported in %-deviation from the reported values of the standard reference material ECRM 752-1 (n = 3) (Greaves et al., 2005) and equals 7% for this

analytical session. Precision is reported in relative standard deviation; % RSD of the ECRM 752 carbonate reference material (n= 3) is better than 1% for Mn/Ca

2.7. Stable oxygen and carbon isotopes

We used nine HAW, nine HAO and ten HL for stable isotope measurements. About 100 µg of sample powder was transferred to borosilicate glass tubes and sealed with plastic caps. Each sample was measured three times.

Stable isotopes were measured at Goethe University Frankfurt on a Thermo MAT 253 Mass Spectrometer interfaced with a Thermo Fisher Scientific GasBench II. The sample material (100 µg) was reacted with 99% H_3PO_4 at 72°C in continuous flow mode. Analytical procedures followed Spötl and Vennemann (2003). $\delta^{13}C$ and $\delta^{18}O$ values are reported in δ-notation, i.e. ‰-deviation relative to Vienna Pee Dee Belemnite (VPDB) and Vienna Standard Mean Ocean (VSMOW), respectively. Internal precision is better than 0.06‰ ($\delta^{13}C$) and 0.08‰ ($\delta^{18}O$).

Samples of the ambient water were collected during scientific cruise POS525 with R/V *Poseidon* in July 2018 (Büscher, 2018; GEOMAR Helmholtz-Zentrum für Ozeanforschung, 2015). A Rosette Sampler equipped with conductivity, temperature and depth sensors (CTD, Sea-Bird Scientific. SBE 911 Plus) was used to sample water from the investigated reefs. The water samples were transferred from 12 L Niskin bottles to 250 mL borosilicate bottles and sealed after adding 100 µL $HgCl_2$ to prevent biological activity of microorganisms that may alter the isotopic composition. The samples were stored in a fridge at 4°C until measurement.

Water samples were analyzed for their isotopic composition at Friedrich-Alexander University Erlangen-Nürnberg by an automated equilibration unit (Gasbench II; Thermo Fisher Scientific) coupled in continuous flow mode to a Delta *plus* XP isotope ratio mass spectrometer (Thermo Fisher Scientific, Bremen, Germany).

Water for $\delta^{13}C$ analyses was extracted from the sample bottles by a 1-mL disposable syringe through the septa without opening the bottle to avoid loss of CO_2 during sample transfer. During water extraction, the removed volume was simultaneously replaced by inert gas through a second needle connected to an argon-filled gas sampling bag (Grace, Deerfield, IL, USA). The samples were injected into 12 mL Labco Exetainers™ (Labco Ltd. Lampeter, U.K) that were prepared with phosphoric acid and pre-flushed with helium (purity 99.999%). For seawater the injection volume was 0.85 mL per vial. Samples were analyzed in duplicates and the reported values are arithmetic means. All values are reported in the standard δ-notation in per mille (‰) vs. VPDB.

Sample bottles for $\delta^{18}O$ were de-capped and 0.5 mL water were extracted with a pipette for CO_2 equilibration. The samples were transferred into 12 mL Labco Exetainers™ (Labco Ltd. Lampeter, U.K) and subsequently flushed with 0.3% CO_2 in helium. Equilibration time was 24 hours at 25 °C. All samples were measured in duplicates and the reported values are arithmetic means. All values are reported in the standard δ-notation in per mille (‰) vs. VSMOW. External reproducibility based on repeated analysis of control samples was better than 0.1‰ and 0.05‰ for $\delta^{13}C$ and $\delta^{18}O$, respectively.

2.8. Statistical computation

We used one-way ANOVA to test the effect of the host species on the elemental and isotopic composition in *H. sarcophaga*. Shapiro-Wilk test and Levene's test were used to ensure normal distribution and equal variance of the target variables. Most groups and target variables are normally distributed except for Na/Ca in the HAO group and $\delta^{18}O$ in the HL group. All target variables except for Mn/Ca and Sr/Ca show equal variance based on the Levene's test. Normal distribution and equal variance are considered a prerequisite for ANOVA. As these prerequisites are not met in some sample groups, we additionally tested the data with a Kruskal-Wallis test which is a non-parametric alternative to ANOVA (Lantz, 2013). Pairwise comparison of the different groups was accomplished with Bonferroni adjusted Tuckey-HSD test. All reported *p*-values are Bonferroni adjusted.

3. Results

3.1. Carbonate Polymorph

The investigated *H. sarcophaga* samples show no staining (Supplement S1) under the influence of cobalt nitrate solution. Consequently, the shells are calcitic as is the case for other species of the order Rotaliida (Horton et al., 2021).

3.2. Fluorescence microscopy

The fluorescence microscopic image of *H. sarcophaga* attached to *A. excavata* (Fig. 1) shows distinct fluorescent and non-fluorescent layers in the shell repair zone (SRZ) of the bivalve. Highly fluorescent material is also observable on *H. sarcophaga*, especially in the test apertures.

The SRZ has a maximum thickness of 900 µm, decreasing in all directions. The fluorescent layers in the SRZ are 20 – 40 µm thick. These layers taper off distally from the bore canal and disappear. Non-fluorescent layers are generally smaller ranging from 9- 20 µm. The asymmetric pit that is produced by the foraminifera is observable, one side of the pit is rising steeply whereas the other side has a shallower angle. The bore canal, which starts at the bottom of the attachment etching, is 400 µm long in the undisturbed bivalve shell, but continues in the callus by another 240 µm. At the start of the bore

the canal is 340 µm in diameter and continuously narrows to 140 µm. The canal ends in the SRZ with a "mushroom-like" shape.

3.3. Element composition of point measurements (EPMA)

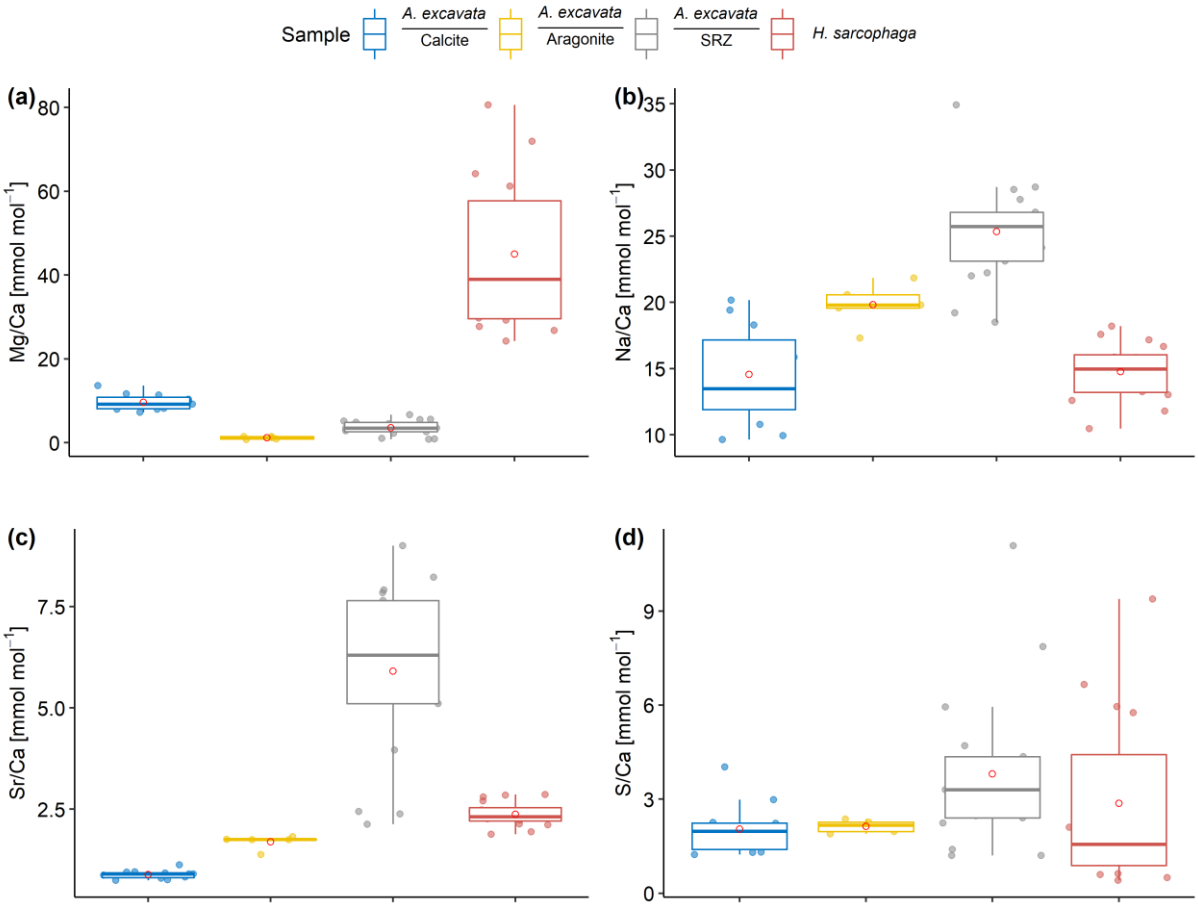

Figure 2 Results of point measurements by EPMA in different sections of *A. excavata* and *H. sarcophaga* (two specimens each). A: Mg/Ca, B: Na/Ca, C: Sr/Ca, D: S/Ca. Boxes display the interquartile range (IQR) and lines the median values. The whiskers show min and max values that are within the range of Q1- 1.5*IQR - Q3 + 1.5*IQR. Red circles show the mean values. Sample size = 11, 5, 17, 16 (Calcite, Aragonite, SRZ, *H. Sarcophaga*). Text below the horizontal lines in the legend is the sampled area.

Table 1 Wilcoxon-Mann-Whitney test results of E/Ca comparison between the observed shell sections. Bold fields show significant differences between the two groups. *p*-values are Bonferroni adjusted.

Wilcoxon-Mann-Whitney Test			
	Group 1	**Group 2**	***p***
Mg/Ca	**Calcite**	**Aragonite**	**0.003**
	Calcite	**SRZ**	**<0.001**
	Calcite	***H. sarcophaga***	**<0.001**
	Aragonite	SRZ	0.051
	Aragonite	***H. sarcophaga***	**<0.001**
	SRZ	***H. sarcophaga***	**<0.001**
Na/Ca	Calcite	Aragonite	0.052
	Calcite	**SRZ**	**<0.001**
	Calcite	*H. sarcophaga*	1

	Aragonite	**SRZ**	**0.027**
	Aragonite	***H. sarcophaga***	**0.002**
	SRZ	***H. sarcophaga***	**<0.001**
Sr/Ca	**Calcite**	**Aragonite**	**0.003**
	Calcite	**SRZ**	**<0.001**
	Calcite	***H. sarcophaga***	**<0.001**
	Aragonite	**SRZ**	**<0.001**
	Aragonite	***H. sarcophaga***	**<0.001**
	SRZ	***H. sarcophaga***	**<0.001**
S/Ca	Calcite	Aragonite	1
	Calcite	SRZ	0.116
	Calcite	*H. sarcophaga*	1
	Aragonite	SRZ	0.286
	Aragonite	*H. sarcophaga*	1
	SRZ	*H. sarcophaga*	0.66

Within the bivalve shell Mg/Ca varies between 0.2 and 13.7 mmol mol^{-1} (Fig. 2). Lowest values were found in the aragonitic shell layer (Fig 1/E_3) and highest values are measured in the microgranular calcitic shell layer (Fig 1/E_2). The highest Mg/Ca ratios are measured in the foraminiferal calcite (mean = 45.0 ± 17.9 mmol mol^{-1}, max = 80.6 mmol mol^{-1}).

Na/Ca ratio are characterized by similar values in the different sections when considering the carbonate polymorph, that they are built of. The aragonitic sections (Fig 1/E_3), bivalve aragonite and SRZ, have mean Na/Ca ratios of 22.0 ± 2.3 mmol mol^{-1} (mean ± sd) and 25.3 ± 3.8 mmol mol^{-1} respectively. The SRZ displays a higher variability than the undisturbed aragonite. The microgranular calcite is characterised by a mean Na/Ca of 14.8 ± SD = 3.7 mmol mol^{-1} (Fig 1/E_2).

The SRZ is enriched in Sr/Ca compared to the undisturbed shell sections. Mean ratios are nearly four times higher than in the undisturbed aragonitic shell parts (5.9 ± 2.1 mmol mol^{-1} compared to 1.5 ± 0.2 mmol mol^{-1}). Lowest values are measured in the bivalve's microgranular calcite (mean = 0.9 ± 0.1 mmol mol^{-1}).

S/Ca ratios are comparable in the undisturbed bivalve aragonite and microgranular calcite, with 1.9 ± 0.3 mmol mol^{-1} and 2.1 mmol mol^{-1} ± 0.8 mmol mol^{-1}, respectively. Similar to Sr/Ca, the highest mean and maximum S/Ca ratios are measured in the SRZ (mean = 3.8 ± 2.5 mmol mol^{-1}, max = 11.1 mmol mol^{-1}. However, all these differences are insignificant (Table 1).

Elemental composition of the SRZ

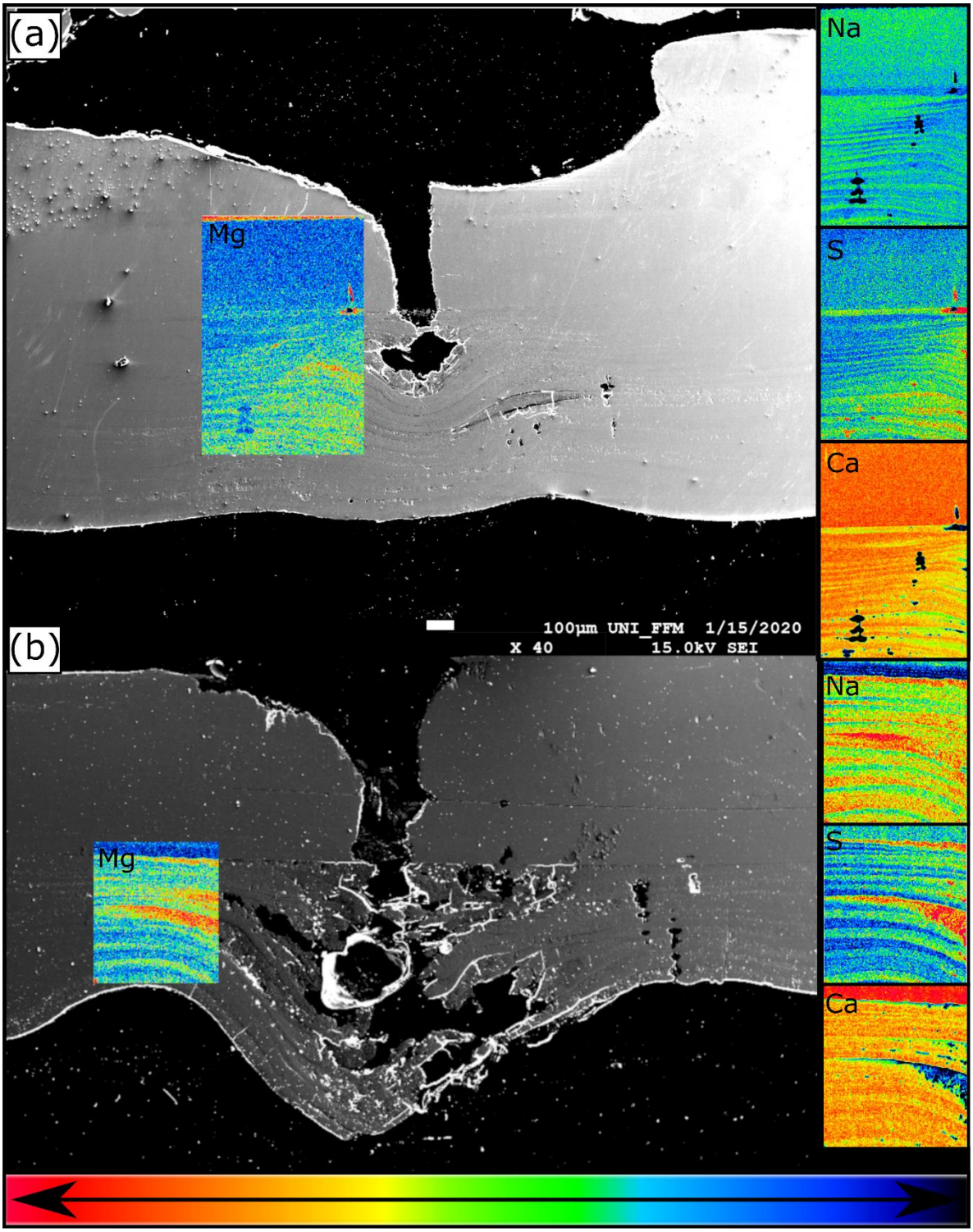

Figure 3 EPMA element maps and secondary-electron image from an SEM of the callus area of two specimen (A & B) of *A. excavata*. Intensity scale in counts per second (cps). Min-Max counts amount to: Mg (10-24 cps), Na (76-132 cps) Ca (7600-8650 cps), S (8.5-33)

As also visible in the fluorescence image (Fig. 1), the EPMA chemical maps show a layering pattern (Fig. 3). Highly fluorescent layers, that coincide with Mg and S maxima and Ca minima are variable in size

ranging from 15 to 80 µm in thickness. Non-fluorescent layers that coincide with Mg and S minima and Ca maxima are more uniform in size, ranging from 12.5 to 30 µm in thickness. Mean composition of the fluorescent (fl) and non-fluorescent (nfl) layers, based on EPMA point measurements amount to: fl: Mg/Ca = 3.8 mmol mol^{-1} ± 1.7 mmol mol^{-1}, Sr/Ca = 7.4 mmol mol^{-1} ± 1.2 mmol mol^{-1}, Na/Ca = 24.4 mmol mol^{-1} ± 5.4 mmol mol^{-1}, S/Ca = 5.5 mmol mol^{-1} ± 2.7 mmol mol^{-1}; nfl: Mg/Ca = 3.2 mmol mol^{-1} ± 1.8 mmol mol^{-1}, Sr/Ca = 4.6 mmol mol^{-1} ± 1.9 mmol mol^{-1}, Na/Ca = 26.6 mmol mol^{-1} ± 1.3 mmol mol^{-1}, S/Ca = 2.3 mmol mol^{-1} ± 0.9 mmol mol^{-1}. Significant mean differences between fluorescent and non-fluorescent layers, based on Wilcoxon-Mann-Whitney test, are evident with regards to the S/Ca (p<0.001) and Sr/Ca ratios (p=0.006).

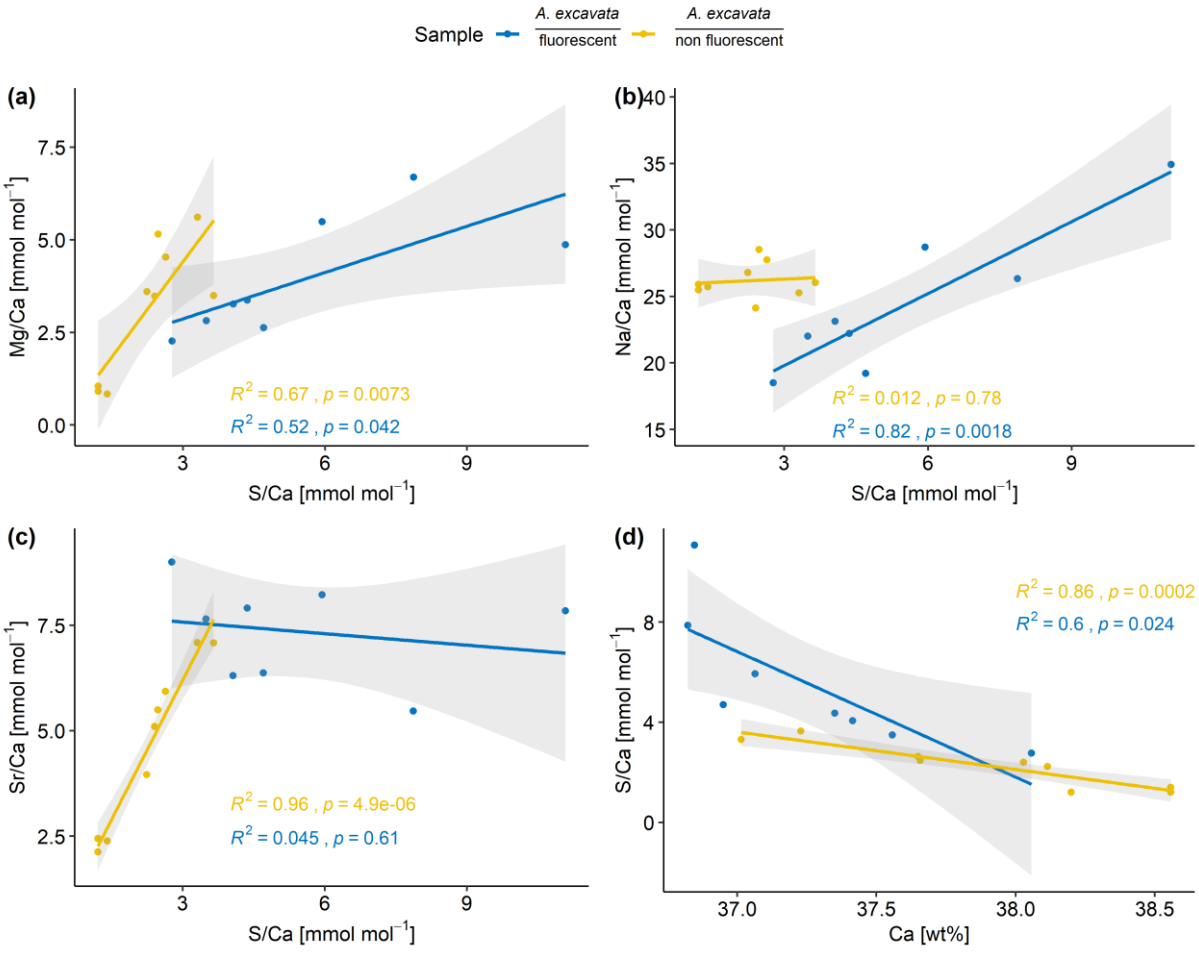

Figure 4 Elemental composition of the SRZ divided according to their fluorescence. Linear correlations are shown for both layers with 95% confidence intervals in gray.

Mg/Ca and S/Ca as well as Na/Ca and S/Ca display significant correlations in the fluorescent layers (Fig. 4). In the non-fluorescent shell layers, Mg/Ca and S/Ca, Sr/Ca and S/Ca are significantly correlated. In both layers, S/Ca ratios are inverse correlated with Ca wt% (Fig. 4).

3.4. Stable carbon and oxygen isotope

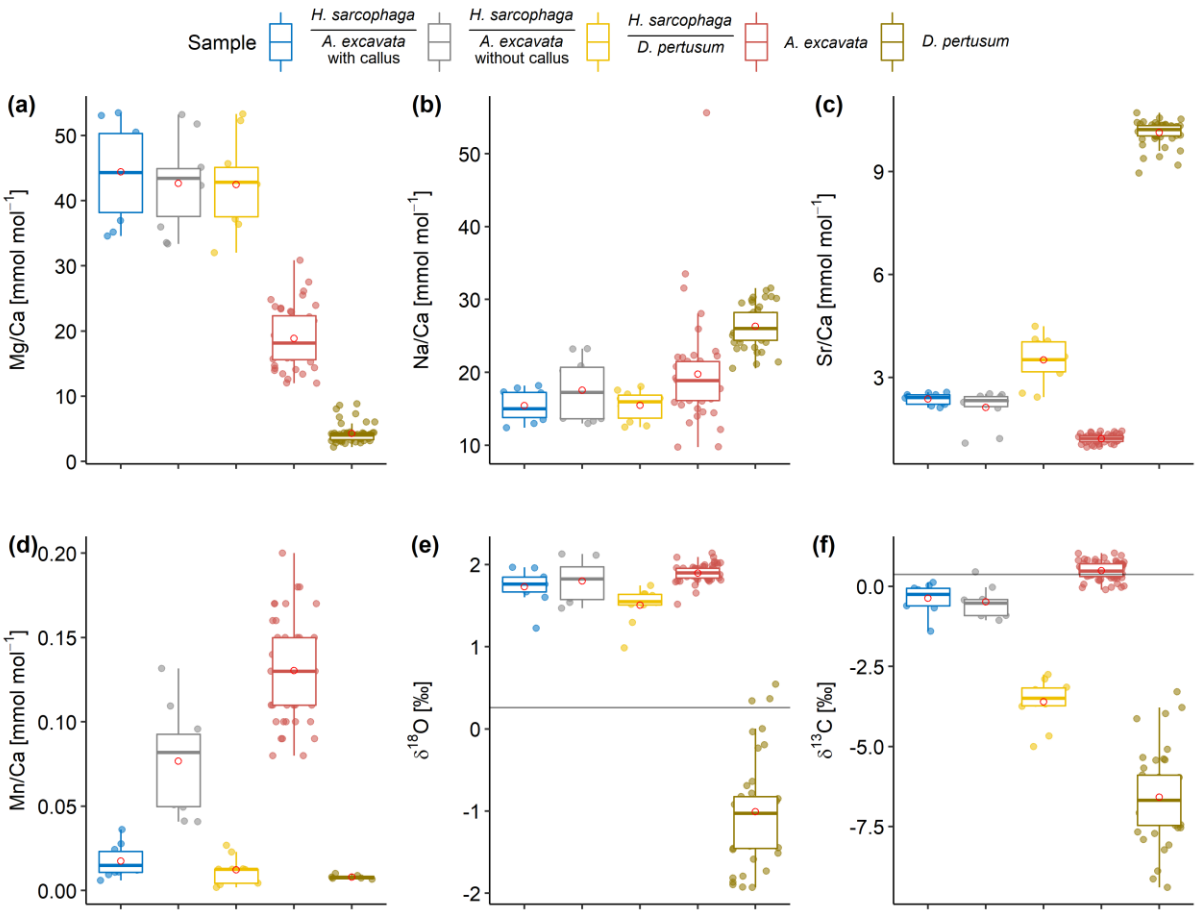

Figure 5 Box- and whisker plots displaying the E/Ca (ICP-OES and ICP-MS) and stable isotope analysis (MS) of the investigated specimens. Boxes display the interquartile range and lines the median values. The whiskers show min and max values that are within the range of Q1- 1.5*IQR - Q3 + 1.5*IQR. Red circles show mean values. Lines in E and F show the isotopic composition of the ambient seawater. Text below the horizontal lines in the legend is the host organism that *H. sarcophaga* grew on.

The different *H. sarcophaga* shells exhibit differences in their isotopic composition based on their host organism (Fig. 4 E/F). In particular, $\delta^{18}O$ values are similar in HL and HA with +1.51 ± 0.22 ‰ and +1.80 ± 0.25 ‰, respectively. These values are in accordance with $\delta^{18}O$ values from the host organism *A. excavata*, which range from +1.52 ‰ to +2.1 ‰. *D. pertusum* displays more depleted $\delta^{18}O$ and $\delta^{13C}C$ values, ranging from -1.93 ‰ to +0.54 ‰ and -9.41 ‰ to -3.30 ‰.

Larger differences between the different *H. sarcophaga* samples are observable in the carbon isotopic signature of specimens taken from different host organisms. HA display $\delta^{13}C$ values of -0.43 ± 0.47 ‰ which is close to the ratios of their host organism, being +0.49 ± 0.28 ‰. HL are more depleted in heavy carbon isotopes with a measured value of -3.61 ± 0.71 ‰. For reference, the isotopic composition of the ambient seawater is $\delta^{18}O$ = +0.26 ‰ and $\delta^{13}C$ = +0.38 ‰.

The isotopic composition of HAW and HAO can be described by linear functions whereas the isotopic composition in HL cannot:

$\delta^{13}C_{HAW} = 1.8\pm0.4 * \delta^{18}O - 3.4\pm0.8$ ($r^2 = 0.7$, p=0.004, df = 7) [1]

$\delta^{13}C_{HAO} = 1.1\pm0.3 * \delta^{18}O - 2.6\pm0.6$ ($r^2 = 0.6$, p=0.02, df = 6) [2]

$\delta^{13}C_{HL} = 1.7\pm1.0 * \delta^{18}O - 6.2\pm1.5$ ($r^2 = 0.18$, p=0.12, df = 8) [3]

3.5. ICP-OES results from *H. sarcophaga* grown on different host organisms

H. sarcophaga samples from different host organisms are similar in their chemical composition with regard to Mg/Ca and Na/Ca (Fig. 5 A/B). Mean Mg/Ca ratios range from 42.7 ± 6.8 to 44.4 ± 7.2 mmol mol^{-1}. Both host organisms have lower mean Mg/Ca ratios of 4.3 ± 1.5 mmol $mol^{-1}$and 18.9 ± 4.5 mmol mol^{-1} in *D. pertusum* and *A. excavata*, respectively.

Mean Na/Ca ratios range between 15.4 ± 2.1 to 17.6 ± 4.3 mmol mol^{-1} for *H. sarcophaga*. The highest Na/Ca ratios and variations are measured in HAO. *D. pertusum* displays overall higher Na/Ca ratios than *H. sarcophaga* (26.3 ± 2.8 mmol mol^{-1}). The highest variation is measured in *A. excavata* ranging from 9.8 to 55.6 mmol $mol^{-1}$with a mean of 19.8 ± 7.3 mmol mol^{-1}.

A clear difference in Sr/Ca of 1.1 ± 0.16 mmol mol^{-1} is evident between *H. sarcophaga* from the different host organisms (Fig. 5 C). HAW and HAO show mean Sr/Ca ratios of 2.4 ± 0.2 and 2.1 ± 0.5 mmol mol^{-1}, respectively. The host organism *A. excavata* has lower Sr/Ca ratios (1.2 ± 0.1 mmol mol^{-1}). On the contrary, HL and *D. pertusum*, display higher mean Sr/Ca ratios of 3.5 ± 0.7 and 10.13 ± 0.3 mmol mol^{-1} respectively.

Prominent differences between *H. sarcophaga* groups are also evident in their Mn/Ca ratios (Fig. 5 D). HAW, HL and *D. pertusum* display Mn/Ca ratios of 0.017 ± 0.01 mmol mol^{-1}, 0.012 ± 0.008 mmol mol^{-1} and 0.008 ± 0.001 mmol mol^{-1}, whereas HAO and *A. excavata* show higher Mn/Ca ratios of 0.077 ± 0.03 mmol mol^{-1} and 0.13 ± 0.03 mmol mol^{-1}, respectively.

3.6. Compositional differences in *H. sarcophaga* related to their host organism

Table 2 Results of the one-way ANOVA and Kruskal-Wallis analysis with the host organism as predictor variable. Bold fields show elemental and isotopic ratios in *H. sarcophaga* that may be significantly influenced by the chemistry of the host organism. *p*-values are Bonferroni adjusted.

	ANOVA					
	Mg/Ca	Na/Ca	**Sr/Ca**	**Mn/Ca**	**$\delta^{18}O$**	**$\delta^{13}C$**
DFn			2			
DFd			25			
F	0.2	0.22	23	32	4.1	97
p	0.82	0.8	**<0.001**	**<0.001**	**0.029**	**<0.001**
Generalized eta squared	0.015	0.018	0.65	0.74	0.26	0.89

Kruskal-Wallis test						
n	28					
df	2					
p	0.83	0.92	**<0.001**	**<0.001**	**0.03**	**<0.001**

We conducted a one-way ANOVA and Kruskal-Wallis test (Table 2) in order to explore if the investigated *H. sarcophaga* groups (HAW, HAO, HL) show significant differences in their geochemical composition related to their host organism. We used the measured elemental and isotopic composition as target variables and the host organisms (*A. excavata* with callus, *A. excavata* without callus, *D. pertusum*) as the factor variable. Tukey-HSD (Table 3) was used as post-hoc test to investigate group specific mean differences.

Table 3 Tukey-HSD test results. Bold fields show significant differences between the two groups. HAW = *H. sarcophaga* that infested *A. excavata* with callus formation, HAO 0 *H. sarcophaga* that infested *A. excavata* without callus formation, HL = *H. sarcophaga* that infested *D. pertusum*. *p*-values are Bonferroni adjusted.

Tukey-HSD test				
	Group 1	**Group 2**	**Difference**	***p***
Mg/Ca	HAW	HAO	-1.22	0.93
	HAW	HL	-1.95	0.81
	HAO	HL	-0.73	0.97
Na/Ca	HAW	HAO	0.74	0.81
	HAW	HL	0.05	0.99
	HAO	HL	-0.68	0.84
Sr/Ca	HAW	HAO	-0.004	1
	HAW	**HL**	**1.14**	**<0.001**
	HAO	**HL**	**1.14**	**<0.001**
Mn/Ca	**HAW**	**HAO**	**0.05**	**<0.001**
	HAW	HL	-0.005	0.75
	HAO	**HL**	**-0.05**	**<0.001**
$\delta^{18}O$	HAW	HAO	0.07	0.81
	HAW	HL	-0.23	0.11
	HAO	**HL**	**-0.30**	**0.032**
$\delta^{13}C$	HAW	HAO	-0.11	0.91
	HAW	**HL**	**-3.24**	**<0.001**
	HAO	**HL**	**-3.12**	**<0.001**

The one-way ANOVA reveals no significant difference in the Mg/Ca and Na/Ca ratios of the foraminifera that were collected from the different host organisms (Table 2). In contrast, the ANOVA suggests a significant difference between Sr/Ca and Mn/Ca ratios between these two groups. In the case of Sr/Ca, significant differences based on the Tukey-HSD post-hoc test are observable between HL and HA, whereas we find no significant differences between HAW and HAO. In addition, we observe no significant differences between HAW and HL in their Mn/Ca composition, but significant differences are present between both these groups and HAO.

In the case of the stable oxygen isotope composition, we observe significant differences between *H. sarcophaga* specimens from different host organisms. The $\delta^{18}O$ measured in HL is significantly lower than in HAO. Significant differences are also observable for $\delta^{13}C$ ratios. Here, differences in the isotopic composition are detectable between HL and HA, with the latter showing higher $\delta^{13}C$ ratio.

The Kruskal-Wallis test, which was used as a non-parametric cross validation for the ANOVA test, shows the same results as the ANOVA test

4. Discussion

4.1. Mechanisms of etching and boring

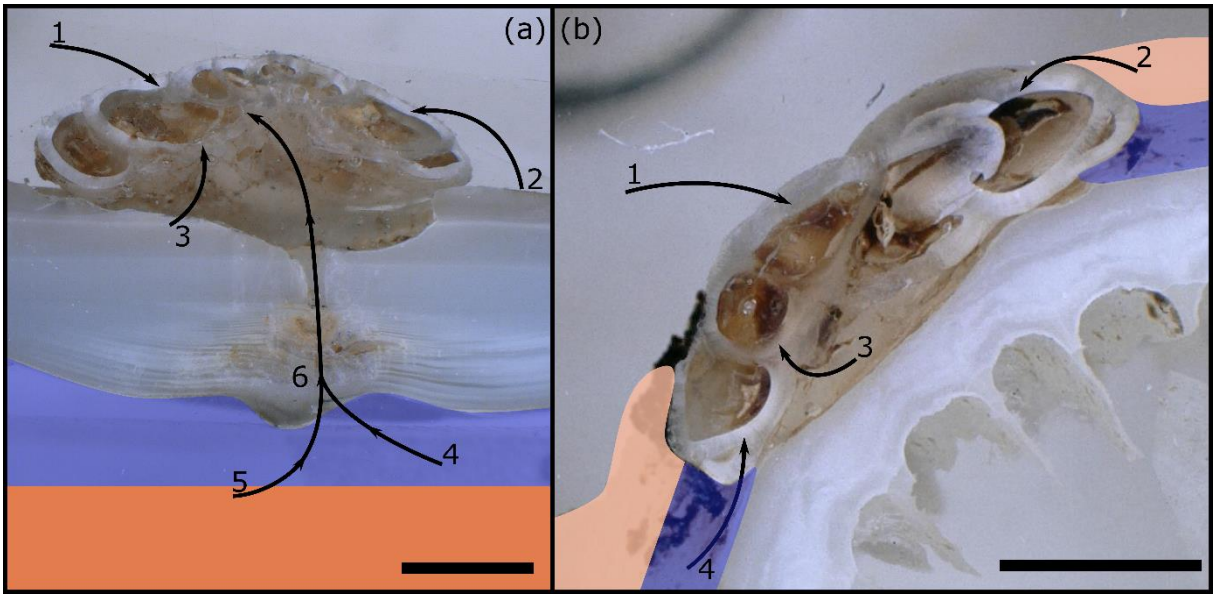

Figure 6 Possible pathways of E/Ca and isotopic signals into the foraminiferal calcite. A: *H. sarcophaga* on *A. excavata*, B: *H. sarcophaga* on *D. pertusum.* Blue areas represent the calcifying space, orange areas represent mantle tissue in *A. excavata* (A) and organic layer (coenosarc/mucus) in *D. pertusum* (B). Uptake of seawater and free-floating particles (1), Ingestion of host organic material (periostracum, coral tissue/mucus) (2), Ingestion of dissolved carbonate material (3), Ingestion of extracellular calcifying fluid (ECF) (4), Ingestion of Mantle tissue (5), ingestion of carbonate and organic material from the deposited callus (6). Scalebar is 100 µm. Please note that the calcifying space and organic layers are displayed enlarged for improved visibility. Actual size of the calcifying space amounts to 1-100 nm (Nakahara, 1991; Tambutté et al., 2007). The organic layer (coenosarc) is ~ 25 µm in thickness (Tambutté et al., 2007).

The boring and etching of *H. sarcophaga* in *A. excavata* and *D. pertusum* can serve multiple purposes. The attachment etchings of foraminifera have been proposed to serve as an anchoring function and increase protection from predators and the hydrodynamic regime. Possibly, the foraminifera also dissolve the host's carbonate material to satisfy the calcium and/or DIC requirements of *H. sarcophaga* for the calcification of its shell (Cedhagen, 1994; Vénec-Peyré, 1996; Todd, 1965), rather than expending further energy to source Ca/DIC from the surrounding seawater (Fig 6A).

The boring in *A. excavata* is presumably produced to access the softbody of the bivalve, indicated by the mantle damage in the vicinity of the boring (Cedhagen, 1994). Additionally, the foraminifera may benefit from ingesting the ECF of the bivalve, containing carbohaydrates, proteins, glycoproteins and

amino acids therefore constituting a valuable nutrient source (Yin et al., 2005). The ECF is also enriched in Ca and CO_2 compared to the ambient seawater, maybe providing additional ions for the calcification of *H. sarcophaga* (Crenshaw, 1972). Feeding on mantle fluids of bivalves by parasitic foraminifera is also supported by tracer experiments on C*. refulgens* (Alexander and Delaca, 1987). With *D. pertusum* as host, the foraminifera can access the coenosarc and underlying calcifying space of the coral without having to bore through the carbonate skeleton (Fig. 6B).

H. sarcophaga probably uses chemical etching, as indicated by the xenoglyph surface texture of the trace that changes in correlation with the host's microstructure (Beuck et al., 2008; Todd, 1965) A possible mechanism was investigated in the non-symbiotic benthic foraminifera *Ammonia* sp., which uses H^+-ATPase to actively pump H^+-ions out of their protoplasm to facilitate calcification (Toyofuku et al., 2017). This proton-flux causes a pH decrease by up to 1.1 in a 100 µm wide zone around the foraminifera (Toyofuku et al., 2017). Similar effects are reported from excavating sponges. *Cliona varians* displays pH values as low as 5 in their filopodia during carbonate dissolution (Webb et al., 2019).

4.2. Sr/Ca differences in *H. sarcophaga* related to the host organism

We observe significant differences in the Sr/Ca and Mn/Ca composition between *H. sarcophaga* from different host organisms.

HL show significantly higher Sr/Ca ratios than HA. Given that this result is based on measurements from multiple individuals distributed across more than one host organism, we suggest that this is most likely a signal of the high Sr/Ca aragonite precipitated from *D. pertusum* that is imprinted into the test of *H. sarcophaga*. By chemically corroding the attachment etching as well as by the penetrating boring and by taking up the resulting solutions, the foraminifera gains access to a pre-concentrated calcium carbonate solution from which it can precipitate its shell (Fig. 6). Naturally, the foraminifera would also reflect other characteristics of the host, such as the high Sr/Ca ratio from the aragonite of *D. pertusum* (Raddatz et al., 2013; Schleinkofer et al., 2019). In agreement with the much lower Sr/Ca ratios in calcite and aragonite in *A. excavata* (Schleinkofer et al., 2021) compared to the coralline aragonite, we do not observe such high Sr/Ca ratios in HA. Still, the observed Sr/Ca ratios in HA are higher by a factor of two than in the host organism. Since we do not observe differences between HAW and HAO, the Sr/Ca surplus cannot be derived from the ingestion of organic material from within the shell cavity. We hypothesis that a possible further control is likely provided through the mixture of dissolved host $CaCO_3$ material and ambient seawater from which the foraminifera calcify, which is explored in more detail in the next section.

4.3. Mixing model

In order to further investigate the observed results, we created a simple two-component model to explore how the trace-element chemistry of *H. sarcophaga* could change by delivery of ions to the calcification site that were derived from dissolution of the host organism. In this model we calculate changes of the foraminifera composition in dependence from an assumed calcification from a variable mixture of seawater and dissolved host carbonate material. We excluded the addition of the hosts calcifying fluid in the model because there is no data available for the chemical composition of the calcifying fluid of *D. pertusum* nor *A. excavata*, and because the model is intended only as an initial exploration of whether the geochemistry of *H. sarcophaga* can be explained by calcification from a mixture of seawater and dissolved host material. Furthermore, measurements of the chemical composition of the calcifying fluid of other bivalve species indicate that the composition is close to the composition of seawater (Wada and Fujinuki, 1976; Crenshaw, 1972).

The model calculates element/Ca ratios based on calcite precipitation from a fluid that is derived from a mix of seawater (transported to the calcification site, see e.g., (Erez, 2003)), and $CaCO_3$ dissolved from the host organism:

$$\frac{E}{Ca_{Hyrrokkin}} = \frac{E_{SW} + \frac{10^R}{M_{Carb}} * \frac{\frac{E}{Ca_{Host}}}{1000}}{Ca_{SW} + \frac{10^R}{M_{Carb}}} * D_E * 1000 \quad [4]$$

Where E_{SW} = element concentration in seawater, E/Ca_{Host} = element/Ca in host carbonate [mmol mol^{-1}], Ca_{SW} = Calcium concentration in seawater (0.010 mol L^{-1}), D_E = Calcite-Water distribution coefficient, M_{Carb} = atomic mass of $CaCO_3$ (100.08 g mol^{-1}) and R = log mixing ratio between carbonate and seawater [g L^{-1}].

Table 4 Parameters used in the proposed model to explore the effects of carbonate and water uptake of *H. sarcophaga* on the shell chemistry. Host element/Ca ratios are derived from this study. D_E^1 & D_E^2 = Distribution coefficient

	Model parameters				
	E_{SW} [mol L^{-1}]	E/Ca_{Acesta} [mmol mol^{-1}]	$E/Ca_{Desmophyllum}$ [mmol mol^{-1}]	D_E^1	D_E^2
Mg	0.053	19	4.2	0.015 (Segev and Erez, 2006)	0.009 (Oomori et al., 1987)
Na	0.450	20	26	0.00028 (Evans et al., 2015)	0.0001 (Füger et al., 2019)
Sr	0.0001	1.2	10.1	0.16 (Raitzsch et al., 2010)	0.2 (Mucci and Morse, 1983; Evans et al., 2015)
Mn	$5*10^{-9}$	0.131	0.008	0.5	10 (Mucci, 1988)

		(van Dijk et al., 2020)

As we have no information about the amount of dissolved material and water that is taken up by *H. sarcophaga*, we modelled it over six orders of magnitude (log dissolved $CaCO_3$/seawater ratios of -4 to +2). The parameters used are reported in Table 4.

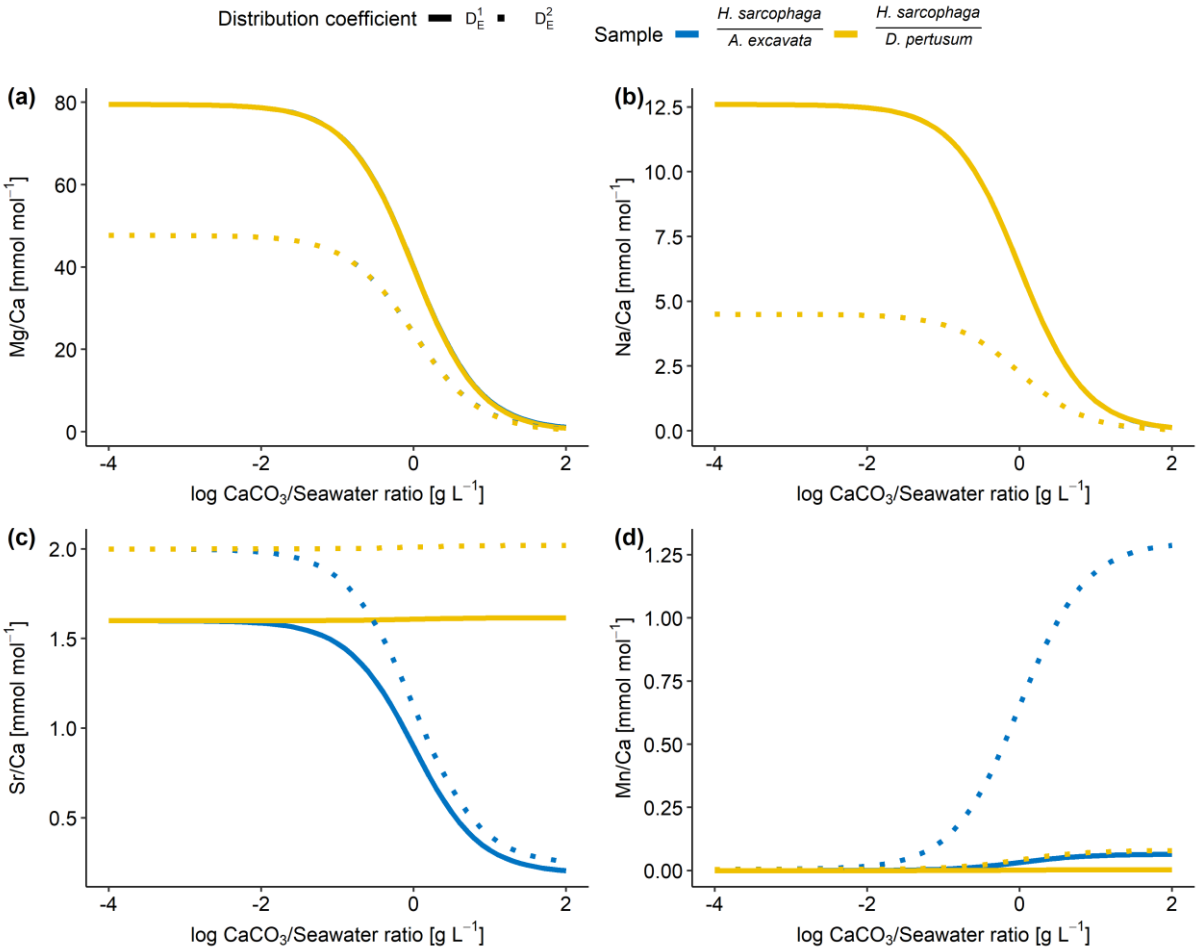

Figure 7 Results of model calculations with the parameters listed in Tab. 4 for the measured E/Ca ratios. Text below the horizontal lines in the legend is the host organism that *H. sarcophaga* grew on. Independently of the mixing ratio of dissolved host $CaCO_3$ and ambient water, no differences of the geochemical signature is predictable in Mg/Ca and Na/Ca. On the contrary, Sr/Ca and Mn/Ca ratios are predicted to diverge at mixing ratios > 0.01 g $CaCO_3$ L^{-1} seawater. Solid lines are produced with D_E^1 for the calculation and dotted lines are produced with D_E^2 for the calculation (see Tab. 4). In panel a and b, the different samples overlap each other.

Based on the model shown in Fig. 7, the Mg/Ca and Na/Ca ratios in *H. sarcophaga* are independent of the geochemical signature of the host it lived on, which is in agreement with our measurements. This is caused by the high concentration of these elements in the ambient seawater in comparison to the host's carbonate. The composition of the mixture is largely controlled by the addition of Ca, which is equal for both host organisms.

In contrast, the model predicts that, at high ratios of $CaCO_3$ derived from the host compared to the surrounding seawater, different Sr/Ca and Mn/Ca ratios should be observed between foraminifera living on different host organisms. The modelled Sr/Ca ratios for HL are constant at 2.0 mmol mol^{-1} independent from the mixing ratio (Fig. 7C). When the foraminifera dissolves aragonitic material of *D. pertusum* and this material is mixed with seawater, the resulting Sr/Ca ratios in this solution do not change due to the aragonitic D_{Sr} being close to 1. Consequently, if the shell Sr/Ca ratio in *H. sarcophaga* depends on calcite D_{Sr} and the Sr/Ca ratio in the calcifying fluid of *H. sarcophaga*, the resulting Sr/Ca ratio in HL is equivalent to a specimen that calcifies solely from seawater (specimen without a host). As the calcitic D_{Sr} is below 1 (Raitzsch et al., 2010; Mucci and Morse, 1983; Evans et al., 2015), the addition of dissolved material from *A. excavata* in the calcifying space results in decreasing Sr/Ca ratios in the calcifying fluid and lower Sr/Ca ratios in the precipitated calcite of the foraminifera. Similar results are obtained in the case of Mn/Ca ratios. The addition of dissolved host material to the calcifying space of *H. sarcophaga* results in an increase of the Mn/Ca ratio in the calcifying fluid, which leads to increasing Mn/Ca ratios in the foraminiferal calcite.

The proposed model can help us understand why we do not see changes in the Mg/Ca and Na/Ca composition of H. sarcophaga from different host organisms and why Sr/Ca and Mn/Ca ratios differ between these groups (Fig. 2). Nonetheless, other processes are clearly required to explain the details of trace element uptake in *H. sarcophaga*. Sr/Ca ratios in HL, for instance, can only be modelled up to 2 mmol mol^{-1}, whereas we measure a mean of 3.5 mmol mol^{-1}. The results of this model are largely driven by the distribution coefficients used, however, the distribution coefficients used in this model are not empirically determined on *H. sarcophaga* but derive from other foraminifera species (D_E[1]) or inorganic precipitation experiments (D_E[2]). The model does also not account for growth-rate driven differences in trace element portioning, while this is especially relevant in the case of Na and Mn (Mucci, 1988; Füger et al., 2019). In addition, we have to consider lattice strain-effects that increase the distribution coefficient for other elements such as Sr and Na, as *H. sarcophaga* has relatively high concentrations of Mg (Evans et al., 2015; Mucci and Morse, 1983).

As discussed above, this is a simplified model that uses seawater and dissolved carbonate as endmembers. An additional possibility is that the foraminifera pumps or channels ions into and out of the calcifying fluid. In particular, it has been suggested foraminifera are able to transport Mg out of the calcifying space (Nehrke et al., 2013; Toyofuku et al., 2017; Bentov and Erez, 2006), but intermediate and high-Mg foraminifera such as *A. lessonii* appear to exert a lower degree of control over the composition of their calcifying fluid compared to low-Mg species (Evans et al., 2018; Geerken et al., 2018). Assuming the calcifying fluid is depleted in Mg in comparison to seawater, the model

would predict lower Mg/Ca ratios, although importantly, it would still not predict a difference in the Mg/Ca ratios of *H. sarcophaga* influenced by the host organism.

Another factor that should be considered is the transport pathway of the dissolved material into the foraminifera's calcifying fluid. The dissolution process of the host organism could modify the chemistry of the ambient seawater in a limited area around the foraminifera (Toyofuku et al., 2017), although this process is hard to imagine in an environment (cold-water coral reef) that relies on constant water movement to provide nutrients to the main inhabitants (Mienis et al., 2007). As such, we suggest it is more likely, that the dissolved material is transported through the cytoplasm to the calcification site (Spero, 1988; Erez, 2003), although further work is required to confirm this.

4.4. Mn/Ca differences in *H. sarcophaga* related to the host organism

Based on the ANOVA analysis (Table 2), significant differences are also observable in the Mn/Ca ratios. HAO display four times higher Mn/Ca ratios then in the other two observed groups. HL show similar Mn/Ca ratios as their host organism, both HAW and HAO show lower Mn/Ca ratios. Based on the differences we observe between the samples that were picked from *A. excavata*, it is unlikely that the Mn/Ca signal in *H. sarcophaga* derives from the host shell material (Fig. 6/A3 & B3). In this case we would expect to see differences between HA and HL as Mn/Ca in *A. excavata* is approximately one order of magnitude higher than in *D. pertusum*. Influences of the surrounding water cannot explain the observed differences either. Manganese, as a redox-sensitive element, is controlled by the oxygen concentration of the ambient water. Under well oxygenated conditions, the main species Mn^{2+} is oxidized to Mn-oxyhydroxides and precipitated (Calvert and Pedersen, 1996, 1993). Low-oxygen conditions lead to a reduction of Mn-oxyhydroxides to the bioavailable Mn^{2+} and a consequent increase of Mn/Ca ratios in biogenic carbonates (Tribovillard et al., 2006; Groeneveld and Filipsson, 2013; Koho et al., 2015). The Leksa Reef, however, is well oxygenated (Milzer et al., 2013; Jacobson, 1983).

An influence of the precipitation rate on Mn/Ca ratio was shown in inorganically precipitated calcite overgrowths and the planktic foraminifera *Orbulina universa* (Mucci, 1988; Lorens, 1981; Holland et al., 2017). Generally speaking, increased calcification rates cause Mn/Ca ratios in the precipitates to decrease (Mucci, 1988; Holland et al., 2017). In our investigated samples, this effect would imply lower calcification rates in HAO compared to HAW and HL. The possibility of HAO having low calcification rates is likely, as it is missing a valuable nutrient source (Fig. 6). Due to the high distribution coefficient of manganese, Rayleigh fractionation might add an additional control on Mn/Ca ratios in the foraminifera shell (Holland et al., 2017). The model of Rayleigh fractionation relies on a number of assumptions about the internal reservoir of the foraminifera regarding the size, initial composition,

refreshment rate and calcification rate (Elderfield, 1996). As these parameters are not fully understood, both for *H. sarcophaga* and foraminifera in general, we cannot provide further information about the possible influence.

A significant influence of the potentially Mn-enriched bodily fluids of bivalves (Wada and Fujinuki, 1976) also cannot explain the differences in the chemical composition as the samples that discern from the others are picked from HAO. These foraminifera did not have access to the internal organic material of the bivalve (Fig. 6/A4). Instead, the high Mn signal in HAO must derive from a source that is located on the outside of the bivalve host (Fig. 6/A2). When the foraminifera initially infests the bivalve and starts boring into the shell, nutrient sources other than the internal organic parts of the bivalve have to be utilised by *H. sarcophaga.* The organic periostracum of the bivalve could depict this nutrient source as it is a highly nutritional source for organic material on the outside of the bivalve's shell (Secor et al., 1993). High concentrations of Mn and Fe were measured in the periostracum of freshwater and marine bivalves (Swinehart and Smith, 1979; Allen, 1960). The mechanistic explanation for this enrichment of Mn and Fe is reported to be the high amount of the amino acids containing glycine and tyrosin in the periostracum of bivalves (Piez, 1961; Whitney et al., 2019), which act as complexing sites for metal ions (Swinehart and Smith, 1979). The existence of living *H. sarcophaga* attached to rocks demonstrates that they do not necessarily rely on a living host but can also supply themselves through other feeding strategies (Cedhagen, 1994). Since algae take up Mn and concentrate it internally (Sunda and Huntsman, 1985), the increased Mn/Ca in HAO could also be caused by a facultative suspension feeding mode of *H. sarcophaga* during its juvenile stage.

At this point we can only speculate about the mechanistic explanation for the enrichment of Mn/Ca in HAO. Future research on *H. sarcophaga* should involve spatially resolved Mn and Fe measurements, to explore if there is an ontogenetic decrease of Mn/Ca ratios in the test of *H. sarcophaga* picked from *A. excavata*. This decrease would mark the time of the first penetration of the bivalve shell.

4.5. Carbonate isotopic composition in *H. sarcophaga* based on the host organism

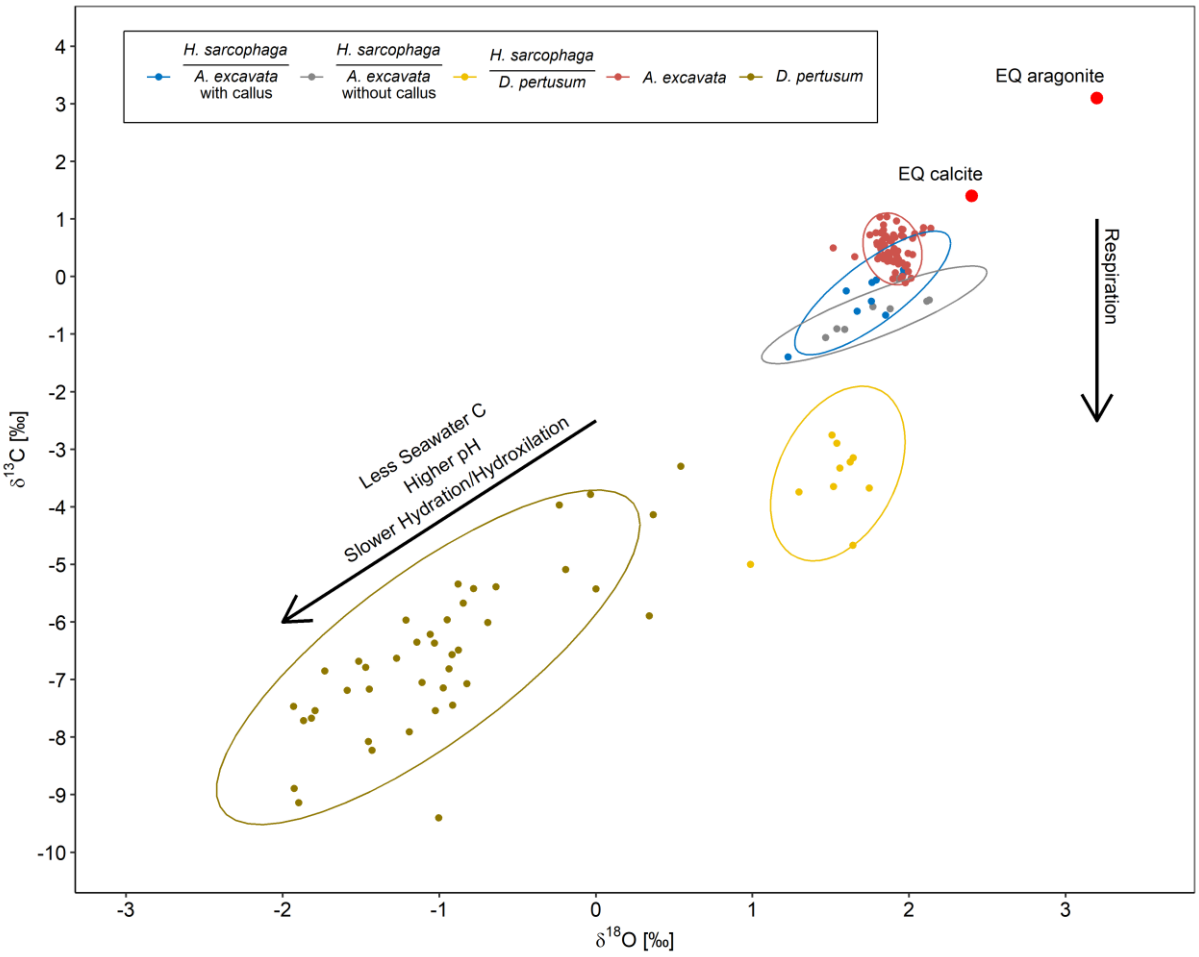

Figure 8 $\delta^{18}O$ plotted against $\delta^{13}C$ for *H. sarcophaga* from different host organisms and the host organisms *A. excavata* and *D. pertusum* with 95 % confidence ellipse. Arrows show compositional changes induced by kinetic effects and respiration. Text below the horizontal lines in the legend is the host organism that *H. sarcophaga* grew on. Red points show the equilibrium composition for calcite and aragonite as calculated from the isotopic composition of the ambient seawater.

The oxygen and carbon isotopic composition of the different organisms are characterised by large differences. *A. excavata* does not show signs of kinetic effects which would be indicated by a correlation of $\delta^{13}C$ and $\delta^{18}O$ values (McConnaughey, 2003; Adkins et al., 2003; Bajnai et al., 2018). Bivalves are largely considered to calcify in equilibrium with the surrounding water (Immenhauser et al., 2016), which appears to be valid for *A. excavata* as it displays an isotopic composition close to the expected equilibrium (Fig. 8). The host organism *D. pertusum* displays higher departures from the expected aragonite equilibrium, which is mainly caused by additional incorporation of isotopically lighter, metabolic CO_2 and by kinetic isotope effects associated with hydration/hydroxylation reactions given that this coral raises the calcification site pH to values significantly exceeding seawater pH (Chen et al., 2018; McCulloch et al., 2012).

Interestingly, the *HA* samples display an isotopic composition very similar to the composition of its host organism (Fig. 8). The 95 % confidence ellipsoids of HAW, HAO and *A. excavata* all overlap at highest $\delta^{18}O$ values. However, in contrast to *A. excavata,* HAW and HAO display positive correlations

between $\delta^{18}O$ and $\delta^{13}C$. This may indicate that all three organisms closely mineralize their carbon from the same source, but hydration/hydroxylation kinetics occur more pronounced in HAW and HAO relative to *A. excavata.*

The observable differences in the carbon isotopic composition between HA and HL can also be caused by different proportions of the carbon sources. HL presumably have constant access to the host's carbon pool, whereas the access of HA to the host's carbon pool is limited due to the defence mechanism of *A. excavata* (Fig. 3). When the bivalve has successfully closed the boring of the foraminifera, the foraminifera must use seawater DIC as a carbon source until it penetrates the shell again. This mixing of different carbon sources in HA in contrast to the stable carbon source of HL can explain the lower $\delta^{13}C$ values in HL due to an increased influence of host derived carbon.

HL is characterized by significantly more positive $\delta^{18}O$ values than its host, and is also characterized by a slightly steeper positive correlation between $\delta^{13}C$ and $\delta^{18}O$. Both circumstances point to faster hydration/hydroxylation kinetics to be effective during the mineralization of HL compared to its host (Chen et al., 2018). If the pH at which HA precipitates carbonate is lower than the pH of the calcifying fluid in *D. pertusum*, the hydration kinetics would be accelerated as a result (Raddatz et al., 2014; Cohen, 2003; Crenshaw, 1972). Both organisms may derive their carbon from the same source which likely occurs depleted in ^{13}C relative to seawater, possibly due to significant admixture from metabolic CO_2. This assertion is supported by the fact that HL has constant access to the host's carbon pool.

Another mechanism potentially altering the $\delta^{13}C$ from equilibrium might be the etching mechanism that pumps H^+-ions in the ambient water around the foraminifera (Toyofuku et al., 2017). The decreasing pH around the foraminifera shifts the carbon speciation towards CO_2. As CO_2 is depleted in ^{13}C compared to the total inorganic carbon pool, the utilization of CO_2 for calcification would also explain the deviations of the foraminifera's shell $\delta^{13}C$ from isotopic equilibrium (Toyofuku et al., 2017; McCorkle et al., 1997).

4.6. Implications for paleoceanographic reconstructions

The results presented here have implications for paleoreconstructions in two ways. When using bivalves for paleo reconstructions or geochemical investigations in general, the shells must be carefully examined for potential traces of bioerosion. In case of callus formation, the carbonate formed can have a significantly different composition than the original carbonate mineralogy.

Even more critical are the implications for paleoceanographic reconstructions using foraminifera which are regularly analyzed for this purpose. Several foraminifera species are known to live on different host organisms and act as parasites and/or bioeroders (Walker et al., 2017; Dupuy et al., 2010; Freiwald and Schönfeld, 1996). Some of these are also used for isotope and element based paleoenvironmental

reconstructions or geochemical investigations in general, such as *Cibicides refulgens* (Mackensen and Nam, 2014; Rathburn and de Deckker, 1997; García-Gallardo et al., 2017), *Hanzawaia concentrica* (Smith and Emiliani, 1968) and *Discanomalia coronata* (Baranwal et al., 2014).

As an example, we use a $\delta^{18}O$-temperature conversion formula for benthic foraminifera (Marchitto et al., 2014) and our measured $\delta^{18}O$ ratios to reconstruct a temperature for the Leksa Reef of 7.5 °C using HAO and 7.8 °C using HAW with $\delta^{18}O_{SW}$ derived from seawater measurements. *In-situ* measurements of the water temperature in the Leksa Reef by CTD show a mean temperature of 7.8°C (min= 7.1°C, max=8.8°C) (Büscher, 2018). If we however use $\delta^{18}O$ ratios from HL we would reconstruct a water temperature of 8.8°C and consequently overestimate the water temperature by 1.0 °C

If the aforementioned species show similar host specific alterations of their isotopic and elemental composition, paleotemperature reconstructions on the basis of these species could be biased. Given that our results indicate that host specific isotopic and elemental composition changes can be present in the parasitic foraminifera *H. sarcophaga* we draw attention to other parasitic foraminifera that should be investigated for similar host-parasite relations, especially if they are used for geochemical investigations.

4.7. Chemical composition of *H. sarcophaga* compared to other benthic foraminifera

H. sarcophaga displays significantly higher Mg/Ca ratios than most other benthic foraminifera species with comparable ecology, that show Mg/Ca ratios between 0.5 and 10 mmol/mol (Lear et al., 2002). Foraminifera that have comparable Mg/Ca ratios to *H. sarcophaga* include *Amphistegina* (23- 77 mmol mol^{-1} (van Dijk et al., 2019; Raja et al., 2005; Geerken et al., 2018)), *Quinqueloculina* (50 – 135 mmol mol^{-1} (Gussone et al., 2016; Toyofuku et al., 2000)) and *Pyrgo* (4 – 85 mmol mol^{-1} (Gussone et al., 2016)) but these species are biologically and mineralogically distinct from *H. sarcophaga. Quinqueloculina* and *Pyrgo* are porcelaneous, whereas *H. sarcophaga* is hyaline. Furthermore, *H. sarcophaga* is not inhabited by photosymbionts in contrast to *Amphistegina*.

The exact processes involved in ion transportation, seawater vacuolization and pH-regulation utilized by *H. sarcophaga* remain to be discovered. High Mg/Ca ratios in *H. sarcophaga* that are similar to inorganic precipitated calcite (Oomori et al., 1987; Mucci and Morse, 1983) may indicate a calcification mechanism without ways of discriminating against elements such as magnesium. These species rely on an increase of the calcification site pH (Erez, 2003; de Nooijer et al., 2009; Toyofuku et al., 2017) to facilitate calcification. The main control on calcite Mg/Ca ratios is then provided by the composition of the calcifying fluid (Raitzsch et al., 2010). The high Mg content would therefore indicate a calcifying space that is more similar to ambient seawater i.e. with no or minor modification via ion channels or pumps (de Nooijer et al., 2014; Bentov and Erez, 2006). Additionally, high Mg/Ca ratios in the calcifying

609 space might be necessary for the stabilization of ACC, a suggested metastable calcite precursor phase
610 in foraminifera and other calcifying organisms (Addadi et al., 2003; Jacob et al., 2011, 2017). High
611 amounts of Mg in the calcite can also cause lattice strain effects, due to the size difference of Mg and
612 Ca ions that causes lattice distortion(Evans et al., 2015; Mucci and Morse, 1983). The lattice distortion
613 can cause an increased incorporation of elements such as Sr and Na (Mucci and Morse, 1983; Evans et
614 al., 2015), a feature that we observe in our samples compared to the species *A. lessonii,* that has slightly
615 lower Mg/Ca ratios than *H. sarcophaga* (35 vs. 45 mmol mol^{-1}) and consequently lower Na/Ca and
616 Sr/Ca ratios (Geerken et al., 2018)

617 **4.8. Biomineralization in the callus region**

618 In order to protect itself from the parasitizing foraminifera, *A. excavata* seals the canal etched through
619 the shell. This is accomplished by rapidly calcifying over the foraminifera boring (Beuck et al., 2008;
620 Cedhagen, 1994). The calcification process produces a callus on the inside of the bivalve shell that is 3-
621 5 mm in diameter and 1-2 mm in height. In the SRZ, evidence can be found for the biomineralization
622 model for bivalves proposed by (Addadi et al., 2006; Checa et al., 2005; Wada and Fujinuki, 1976), i.e.
623 that this process starts with the formation of an organic sheet indicated by the high fluorescence, high
624 S concentration and low Ca concentration of this region, which then acts as a framework during
625 calcification The following layer is depleted in S and enriched in Ca and therefore represents a higher
626 Ca concentration (Fig. 3 & 4). This sequence is repeated multiple times leading to the formation of the
627 visible callus. As long as the foraminifera does not stop the boring process, the bivalve needs to
628 continually counter the boring process by calcifying in the region of infestation.

629 The callus displays high concentrations of organic material that are not observable in the undisturbed
630 regions. The layers that are characterised by high organic contents appear to be preferentially
631 dissolved (Fig. 3B) In cross sections, organic rich areas make up 50 % of the callus (Fig 1D). It appears
632 unlikely that the high amounts of organic material in the SRZ are solely deposited as a calcification
633 framework, considering the differences between undisturbed shell areas and the SRZ. Therefore, the
634 high amount of deposited organic material probably serves some other purpose, such as an increase
635 of the overall material deposition rate and the provision of an initial sealant from the surrounding
636 water.

637 The Boring organisms pose a threat to the bivalve in multiple ways. It has been shown that *H.*
638 *sarcophaga* penetrated the mantle of *A. excavata* which led to a destruction of the mantle epithelium
639 of the bivalve due to ingestion by *H. sarcophaga* (Cedhagen, 1994). Infested sections showed larger
640 numbers of cell nuclei, indicating higher cell division rates and higher metabolic rates (Cedhagen,
641 1994). The pathway through the bivalve shell furthermore allows pathogens to reach and attack the

642 bivalve and could allow surrounding water to permeate into the extra pallial fluid (EPF) of the bivalve.
643 Even though the EPF in several bivalve species shows trace element concentrations close to seawater
644 (Wada and Fujinuki, 1976; Crenshaw, 1972), the bivalve still has to actively concentrate Ca in the
645 calcifying space to reach concentrations that exceed the solubility product (Wilbur and Saleuddin,
646 1983; Bonucci and Wheeler, 2020). This concentration of Ca is accomplished through active pumping
647 by means of enzymes such as Ca-ATPase (Klein et al., 1996) or through ion channels (Carré et al., 2006).
648 In case of an unsealed calcifying space, the dilution with seawater makes high concentrations of Ca-
649 ions to levels needed for calcification in the extra EPF less likely. A fast-sealing method, by means of
650 organic deposition, is therefore necessary to ensure that the bivalve's calcification capability is not
651 compromised.

652 Geochemically, the SRZ shows the largest differences to the undisturbed aragonite in Mg/Ca and Sr/Ca
653 ratios (Fig 2 & 3). Mg/Ca ratios are five times higher in the SRZ than in undisturbed aragonite.
654 Magnesium is thought to be enriched in organic matrices secreted by the bivalve compared to the shell
655 $CaCO_3$ (Schöne et al., 2010). The distribution of magnesium in the SRZ, especially its enrichment in
656 fluorescent layers rich in sulfur (Fig. 1,3 and 4), makes an enrichment of Mg due to high organic
657 concentrations likely. Beside an enrichment of Mg in the secreted organic matter, peptides similar to
658 that found at the site of calcification in bivalves (Moradian-Oldak et al., 1990) can increase the Mg
659 concentration in precipitated calcite by reducing the dehydration enthalpy (Stephenson et al., 2008).
660 These peptides are also regularly found in molluscs (Marin et al., 2007; Falini et al., 1996; Halloran and
661 Donachy, 1995; Zhang and Zhang, 2006). As these peptides do furthermore increase the growth rate
662 by 25 % to 50 % (Stephenson et al., 2008), due to the need of fast calcification (Beuck et al., 2008), it
663 may suggest that a high concentration of peptides in the SRZ is likely. Higher growth rates can
664 additionally lead to an increase of crystal impurities which could alter other elements besides Mg
665 (Lorens, 1981).

666 In contrast to Mg, Sr was not found to be enriched in organic matter compared to shell $CaCO_3$ (Takesue
667 et al., 2008), and therefore the presence of organics cannot explain the observed high Sr/Ca of the
668 aragonite in the SRZ. Yet, there is evidence for the influence of peptides on the incorporation of other
669 elements such as Sr (Stephenson et al., 2008). Sr incorporation in the aragonitic bivalves is considered
670 to be controlled in-part by growth rate effects (Lorrain et al., 2005; Füllenbach et al., 2017; Takesue et
671 al., 2008; Carré et al., 2006). A calcification rate control on Sr incorporation is also supported from
672 abiogenic calcite (Gabitov et al., 2014) but not from abiogenic aragonite (Gabitov et al., 2006).
673 Accordingly, this growth rate effect is probably of biologic nature in aragonite precipitates.

674 Sr likely arrives into the calcifying space via similar pathways as Ca, as was shown by the effects of
675 calcium channel blockers in corals (Ferrier-Pagès et al., 2002). However, Ca-ATPase has a higher affinity

for Ca than Sr (Yu and Inesi, 1995). Therefore, a higher Ca-ATPase activity, as a result of increased growth rates, should lead to decreasing Sr/Ca ratios in the precipitates, which was shown in corals (Ferrier-Pagès et al., 2002; de Villiers et al., 1995). As we expect high growth rates in the SRZ, Ca channels that also transport Sr cannot explain the observed Sr distribution in this zone. Alternatively, the organism's metabolic rate has been suggested to control Sr/Ca in bivalves through metabolic pumping (Klein et al., 1996). High metabolic activity was observed in *A. excavata* infested by *H. sarcophaga,* indicated by a high concentration of cell-nuclei (Cedhagen, 1994). The model of Klein et al. (1996) would predict lower Sr/Ca ratios in these areas, thus a mechanism other than metabolic pumping must control the high Sr/Ca ratios in the SRZ.

Füllenbach et al. (2015) proposed that in slow growing areas of bivalves, the organisms exert less biological control over element incorporation, leading to elevated Sr/Ca ratios. While this hypothesis does not fit to our observation of elevated Sr/Ca ratios in a potentially fast-growing shell area, a similar hypothesis was suggested concerning Mg/Ca in *Mytilus edulis* (Lorens and Bender, 1980). The authors found strongly elevated Mg/Ca ratios in shells sections that were precipitated after handling the specimens for size measurements and attributed this effect to stress (Lorens and Bender, 1980). The boring of *H. sarcophaga* is very likely to be a stress factor on *A. excavata*. An influence of such stress related effects on Mg/Ca and potentially Sr/Ca (Fig. 4) are, therefore, possible. The high Mg-concentrations in the EPF due to a potential breakdown of Mg-regulating mechanisms however, would inhibit the organism from calcification due to the inhibiting effects of Mg on crystal nucleation and growth (Pytkowicz, 1965; Lorens and Bender, 1980). *A. excavata* might circumvent this by releasing additional sulphate bearing organic molecules that provide additional nucleation sites and higher Ca-concentrations at the nucleation sites (Lorens and Bender, 1980), which might potentially be the cause of the observed increased S/Ca ratios in the SRZ (Fig. 4).

5. Conclusion

Our results demonstrate that the elemental and isotopic composition of the parasitic foraminifera *H. sarcophaga* varies depending on the host organisms that the foraminifera settle on. *H. sarcophaga* that lived on the coral *D. pertusum* shows significantly higher Sr/Ca ratios than those that lived on the bivalve *A. excavata*. Combining these data with a simple mixing model, we propose that this could point towards a biomineralization pathway that is influenced by uptake of carbonate material derived from the host. The dissolution of the host shell could serve to satisfy the foraminifera's demand for calcium and DIC.

We also observe significant differences between *H. sarcophaga* specimens that grew on *A. excavata* that can be correlated to the success of the penetration progress. Foraminifera that fully penetrated the bivalve's shell, recognizable by the hosts callus formation, display significantly lower Mn/Ca ratios than foraminifera that did not completely penetrate the shell. This could be an effect of a suspension feeding period of the foraminifera or grazing of Mn-rich material of the periostracum until it penetrated the bivalve's shell when switching to a parasitic mode of feeding. Other possibilities include differences in the growth rate caused by changes of the nutrient availability or Rayleigh fractionation.

The oxygen and carbon isotopic composition of *H. sarcophaga* also appears to be influenced by the type of host organism that it infests. Again, this might be an effect of a direct uptake of the host's organic material and/or $CaCO_3$. Other effects such as different pH regimes in the host organisms and varying equilibration may also play a role. Different extents of the calcification site carbonate system equilibration between *H. sarcophaga* that infested *D. pertusum* (HL) and *H. sarcophaga* that infested *A. excavata* (HA) could also explain the missing signs of kinetic fractionation in HL compared to HA.

As the elemental and isotopic composition of some parasitic foraminifera is used for paleoceanographic reconstructions, our results indicate that such studies should only be performed when the host organism is known.

Author contribution

NS: Investigation**,** Conceptualization, Data curation, formal analysis, Investigation, Visualization, Writing (Original Draft)

DE: Methodology, Formal Analysis, Writing (Review & Editing)

MW: Resources**,** Writing (Review & Editing)

JVB: Resources, Writing (Review & Editing)

JF: Investigation, Resources, Writing (Review & Editing)

AF: Resources, Writing (Review & Editing)

SH: Investigation, Writing (Review & Editing)

HM: Investigation, Resources, Writing (Review & Editing)

SV: Supervision, Resources, Writing (Review & Editing)

JR: Funding Acquisition,Investigation, Project administration, Supervision, Resources, Writing (Review & Editing)

Acknowledgments

We are grateful to all cruise captains, crew members and cruise participants of research cruises POS473 and POS525. We are also grateful for the help of Celestine Beyer and Luciano Zolezzi, who aided with the EPMA measurements. We also want to thank Lennart de Nooijer and Inge van Dijk, whose detailed comments substantially improved our manuscript. This work was funded by the Deutsche Forschungsgemeinschaft, RA 2156-5/1 to JR. This is FIERCE contribution No. 70

Supplements

[1] Pictures of Meigen test

[2] Measurement data

[3] RAW and TIFF pictures of Fig.1

Competing Interests

The authors declare that they have no conflict of interest.

References

Addadi, L., Raz, S., and Weiner, S.: Taking Advantage of Disorder: Amorphous Calcium Carbonate and Its Roles in Biomineralization, Advanced Materials, 15, 959–970, https://doi.org/10.1002/adma.200300381, 2003.

Addadi, L., Joester, D., Nudelman, F., and Weiner, S.: Mollusk Shell Formation: A Source of New Concepts for Understanding Biomineralization Processes, Chemistry - A European Journal, 12, 980–987, https://doi.org/10.1002/chem.200500980, 2006.

Addamo, A. M., Vertino, A., Stolarski, J., García-Jiménez, R., Taviani, M., and Machordom, A.: Merging scleractinian genera: The overwhelming genetic similarity between solitary Desmophyllum and colonial Lophelia, BMC Evolutionary Biology, 16, https://doi.org/10.1186/s12862-016-0654-8, 2016.

Adkins, J. F., Boyle, E. A., Curry, W. B., and Lutringer, A.: Stable isotopes in deep-sea corals and a new mechanism for “vital effects,” Geochimica et Cosmochimica Acta, 67, 1129–1143, https://doi.org/10.1016/S0016-7037(02)01203-6, 2003.

Alexander, S. P. and Delaca, T. E.: Feeding adaptations of the foraminiferan Cibicides refulgens living epizoically and parasitically on the Antarctic scallop Adamussium colbecki, Biological Bulletin, 173, 136–159, https://doi.org/10.2307/1541868, 1987.

765 Allen, J. A.: Manganese deposition on the shells of living molluscs, Nature, 185, 336–337,
766 https://doi.org/10.1038/185336b0, 1960.

767 Bajnai, D., Fiebig, J., Tomašových, A., Milner Garcia, S., Rollion-Bard, C., Raddatz, J., Löffler, N., Primo-
768 Ramos, C., and Brand, U.: Assessing kinetic fractionation in brachiopod calcite using clumped
769 isotopes, Scientific Reports, 8, 533, https://doi.org/10.1038/s41598-017-17353-7, 2018.

770 Baranwal, S., Sauer, S., Knies, J., Chand, S., Jensen, H., and Klug, M.: Benthic foraminifera as tools in
771 interpretation of subsurface hydrocarbon fluid flow at Veslemøy High and Hola-Vesterålen areas of
772 the Barents Sea, Geophysical Research Abstracts, 2014-1843 pp., 2014.

773 Bentov, S. and Erez, J.: Impact of biomineralization processes on the Mg content of foraminiferal
774 shells: A biological perspective, Geochemistry, Geophysics, Geosystems, 7,
775 https://doi.org/10.1029/2005GC001015, 2006.

776 Beuck, L., López Correa, M., and Freiwald, A.: Biogeographical distribution of Hyrrokkin (Rosalinidae,
777 Foraminifera) and its host-specific morphological and textural trace variability, Current
778 Developments in Bioerosion, 329–360, https://doi.org/10.1007/978-3-540-77598-0-17, 2008.

779 Bonucci, E. and Wheeler, A. P.: Mechanisms of Molluscan Shell Formation, in: Calcification in
780 Biological Systems, Plenum Press, 179–216, https://doi.org/10.1201/9781003068396-10, 2020.

781 Büscher, J.: Cold-water coral habitat characterisation and in situ physiological state analyses of four
782 spatially distinct reefs in North- and mid-Norway-Cruise Report RV POSEIDON 525 [POS525],
783 GEOMAR, Kiel, Germany, https://doi.org/10.3289/CR_POS525, 2018.

784 Calvert, S. E. and Pedersen, T. F.: Geochemistry of Recent oxic and anoxic marine sediments:
785 Implications for the geological record, Marine Geology, https://doi.org/10.1016/0025-
786 3227(93)90150-T, 1993.

787 Calvert, S. E. and Pedersen, T. F.: Sedimentary geochemistry of manganese: Implications for the
788 environment of formation of manganiferous black shales, Economic Geology,
789 https://doi.org/10.2113/gsecongeo.91.1.36, 1996.

790 Carré, M., Bentaleb, I., Bruguier, O., Ordinola, E., Barrett, N. T., and Fontugne, M.: Calcification rate
791 influence on trace element concentrations in aragonitic bivalve shells: Evidences and mechanisms,
792 Geochimica et Cosmochimica Acta, 70, 4906–4920, https://doi.org/10.1016/j.gca.2006.07.019, 2006.

793 Cedhagen, T.: Taxonomy and biology of hyrrokkin sarcophaga gen. Et Sp. N., a parasitic foraminiferan
794 (rosalinidae), Sarsia, 79, 65–82, https://doi.org/10.1080/00364827.1994.10413549, 1994.

795 Checa, A. G., Rodríguez-Navarro, A. B., and Esteban-Delgado, F. J.: The nature and formation of
796 calcitic columnar prismatic shell layers in pteriomorphian bivalves, Biomaterials, 26, 6404–6414,
797 https://doi.org/10.1016/j.biomaterials.2005.04.016, 2005.

798 Cheng, Y. R. and Dai, C. F.: A bioeroding foraminifer, Hyrrokkin sarcophaga, on deepwater corals from
799 the South China Sea, Coral Reefs, 35, 901, https://doi.org/10.1007/s00338-016-1447-7, 2016.

800 Chen, S., Gagnon, A. C., and Adkins, J. F.: Carbonic anhydrase, coral calcification and a new model of
801 stable isotope vital effects, Geochimica et Cosmochimica Acta, 236, 179–197,
802 https://doi.org/10.1016/j.gca.2018.02.032, 2018.

803 Cohen, A. L.: Geochemical Perspectives on Coral Mineralization, Reviews in Mineralogy and
804 Geochemistry, 54, 151–187, https://doi.org/10.2113/0540151, 2003.

805 Crenshaw, M. A.: The inorganic composition of molluscan extrapallial fluid, The Biological Bulletin,
806 143, 506–512, https://doi.org/10.2307/1540180, 1972.

807 van Dijk, I., Mouret, A., Cotte, M., le Houedec, S., Oron, S., Reichart, G. J., Reyes-Herrera, J., Filipsson,
808 H. L., and Barras, C.: Chemical Heterogeneity of Mg, Mn, Na, S, and Sr in Benthic Foraminiferal
809 Calcite, Frontiers in Earth Science, 7, 281, https://doi.org/10.3389/feart.2019.00281, 2019.

810 van Dijk, I., de Nooijer, L. J., Barras, C., and Reichart, G. J.: Mn Incorporation in Large Benthic
811 Foraminifera: Differences Between Species and the Impact of pCO2, Frontiers in Earth Science,
812 https://doi.org/10.3389/feart.2020.567701, 2020.

813 Dupuy, C., Rossignol, L., Geslin, E., and Pascal, P. Y.: Predation of mudflat meio-macrofaunal
814 metazoans by a calcareous foraminifer, Ammonia tepida (Cushman, 1926), Journal of Foraminiferal
815 Research, 40, 305–312, https://doi.org/10.2113/gsjfr.40.4.305, 2010.

816 Elderfield, H.: A biomineralization model for the incorporation of trace elements into foraminiferal
817 calcium carbonate, Earth and Planetary Science Letters, 142, 409–423, https://doi.org/10.1016/0012-
818 821X(96)00105-7, 1996.

819 Erez, J.: The Source of Ions for Biomineralization in Foraminifera and Their Implications for
820 Paleoceanographic Proxies, Reviews in Mineralogy and Geochemistry, 54, 115–149,
821 https://doi.org/10.2113/0540115, 2003.

822 Evans, D., Erez, J., Oron, S., and Müller, W.: Mg/Ca-temperature and seawater-test chemistry
823 relationships in the shallow-dwelling large benthic foraminifera Operculina ammonoides, Geochimica
824 et Cosmochimica Acta, 148, 325–342, https://doi.org/10.1016/j.gca.2014.09.039, 2015.

825 Evans, D., Müller, W., and Erez, J.: Assessing foraminifera biomineralisation models through trace
826 element data of cultures under variable seawater chemistry, Geochimica et Cosmochimica Acta, 236,
827 198–217, https://doi.org/10.1016/j.gca.2018.02.048, 2018.

828 Falini, G., Albeck, S., Weiner, S., and Addadi, L.: Control of Aragonite or Calcite Polymorphism by
829 Mollusk Shell Macromolecules, Science, 271, 67–69, https://doi.org/10.1126/science.271.5245.67,
830 1996.

831 Ferrier-Pagès, C., Boisson, F., Allemand, D., and Tambutté, E.: Kinetics of strontium uptake in the
832 scleractinian coral Stylophora pistillata, Marine Ecology Progress Series, 245, 93–100,
833 https://doi.org/10.3354/meps245093, 2002.

834 Form, A. U., Büscher, J. v., Hissmann, K., Flögel, S., Wisshak, M., Rüggeberg, A., Bannister, R., Kutti, T.,
835 Stapp, L., Bennecke, S., Küter, M., Nachtigall, K., Schauer, J., and Fenske, M.: RV POSEIDON Cruise
836 Report POS473 LORELEI II: LOphelia REef Lander Expedition and Investigation II, Tromsø – Bergen –
837 Esbjerg, 15.08. – 31.08. – 04.09.2014., 25 pp., https://doi.org/10.3289/CR_POS_473, 2015.

838 Freiwald, A. and Schönfeld, J.: Substrate pitting and boring pattern of Hyrrokkin sarcophaga
839 Cedhagen, 1994 (Foraminifera) in a modern deep-water coral reef mound, Marine
840 Micropaleontology, 28, 199–207, 1996.

841 Füger, A., Konrad, F., Leis, A., Dietzel, M., and Mavromatis, V.: Effect of growth rate and pH on
842 lithium incorporation in calcite, Geochimica et Cosmochimica Acta, 248, 14–24,
843 https://doi.org/10.1016/j.gca.2018.12.040, 2019.

844 Füllenbach, C. S., Schöne, B. R., Shirai, K., Takahata, N., Ishida, A., and Sano, Y.: Minute co-variations
845 of Sr/Ca ratios and microstructures in the aragonitic shell of Cerastoderma edule (Bivalvia) – Are
846 geochemical variations at the ultra-scale masking potential environmental signals?, Geochimica et
847 Cosmochimica Acta, 205, 256–271, https://doi.org/10.1016/j.gca.2017.02.019, 2017.

848 Gabitov, R. I., Cohen, A. L., Gaetani, G. A., Holcomb, M., and Watson, E. B.: The impact of crystal
849 growth rate on element ratios in aragonite: An experimental approach to understanding vital effects,
850 Geochimica et Cosmochimica Acta, 70, A187, https://doi.org/10.1016/j.gca.2006.06.377, 2006.

851 Gabitov, R. I., Sadekov, A., and Leinweber, A.: Crystal growth rate effect on Mg/Ca and Sr/Ca
852 partitioning between calcite and fluid: An in situ approach, Chemical Geology, 367, 70–82,
853 https://doi.org/10.1016/j.chemgeo.2013.12.019, 2014.

854 García-Gallardo, Á., Grunert, P., Voelker, A. H. L., Mendes, I., and Piller, W. E.: Re-evaluation of the
855 “elevated epifauna” as indicator of Mediterranean Outflow Water in the Gulf of Cadiz using stable

856 isotopes (δ13C, δ18O), Global and Planetary Change, 155, 78–97,
857 https://doi.org/10.1016/j.gloplacha.2017.06.005, 2017.

858 Geerken, E., Jan De Nooijer, L., van DIjk, I., and Reichart, G. J.: Impact of salinity on element
859 incorporation in two benthic foraminiferal species with contrasting magnesium contents,
860 Biogeosciences, 15, 2205–2218, https://doi.org/10.5194/bg-15-2205-2018, 2018.

861 GEOMAR Helmholtz-Zentrum für Ozeanforschung: Research Vessel POSEIDON, Journal of large-scale
862 research facilities JLSRF, 1, 60–63, https://doi.org/10.17815/jlsrf-1-62, 2015.

863 GEOMAR Helmholtz-Zentrum für Ozeanforschung: Manned submersible „JAGO“, Journal of large-
864 scale research facilities JLSRF, 3, 1–12, https://doi.org/10.17815/jlsrf-3-157, 2017.

865 Goldstein, J. I., Newbury, D. E., Michael, J. R., Ritchie, N. W. M., Scott, J. H. J., and Joy, D. C.: Scanning
866 Electron Microscopy and X-Ray Microanalysis, Springer New York, New York, NY,
867 https://doi.org/10.1007/978-1-4939-6676-9, 2018.

868 Goldstein, S. T.: Foraminifera: A biological overview, in: Modern Foraminifera,
869 https://doi.org/10.1007/0-306-48104-9_3, 1999.

870 Gray, W. R. and Evans, D.: Nonthermal Influences on Mg/Ca in Planktonic Foraminifera: A Review of
871 Culture Studies and Application to the Last Glacial Maximum, Paleoceanography and
872 Paleoclimatology, 34, 306–315, https://doi.org/10.1029/2018PA003517, 2019.

873 Greaves, M., Barker, S., Daunt, C., and Elderfield, H.: Accuracy, standardization, and interlaboratory
874 calibration standards for foraminiferal Mg/Ca thermometry, Geochemistry, Geophysics, Geosystems,
875 6, 2–13, https://doi.org/10.1029/2004GC000790, 2005.

876 Greaves, M., Caillon, N., Rebaubier, H., Bartoli, G., Bohaty, S., Cacho, I., Clarke, L., Cooper, M., Daunt,
877 C., Delaney, M., DeMenocal, P., Dutton, A., Eggins, S., Elderfield, H., Garbe-Schoenberg, D., Goddard,
878 E., Green, D., Groeneveld, J., Hastings, D., Hathorne, E., Kimoto, K., Klinkhammer, G., Labeyrie, L., Lea,
879 D. W., Marchitto, T., Martínez-Botí, M. A., Mortyn, P. G., Ni, Y., Nuernberg, D., Paradis, G., Quinn, T.,
880 Rosenthal, Y., Russel, A., Sagawa, T., Sosdian, S., Stott, L., Tachikawa, K., Tappa, E., Thunell, R., and
881 Wilson, P. A.: Interlaboratory comparison study of calibration standards for foraminiferal Mg/Ca
882 thermometry, Geochemistry, Geophysics, Geosystems, 9, 1–27,
883 https://doi.org/10.1029/2008GC001974, 2008.

884 Groeneveld, J. and Filipsson, H. L.: Mg/Ca and Mn/Ca ratios in benthic foraminifera: the potential to
885 reconstruct past variations in temperature and hypoxia in shelf regions, Biogeosciences, 10, 5125–
886 5138, https://doi.org/10.5194/bg-10-5125-2013, 2013.

Gussone, N., Filipsson, H. L., and Kuhnert, H.: Mg/Ca, Sr/Ca and Ca isotope ratios in benthonic foraminifers related to test structure, mineralogy and environmental controls, Geochimica et Cosmochimica Acta, 173, 142–159, https://doi.org/10.1016/j.gca.2015.10.018, 2016.

Halloran, B. A. and Donachy, J. E.: Characterization of organic matrix macromolecules from the shells of the antarctic scallop, Adamussium colbecki, Comparative Biochemistry and Physiology -- Part B: Biochemistry and, 111, 221–231, https://doi.org/10.1016/0305-0491(94)00245-P, 1995.

Hancock, L. G., Walker, S. E., Pérez-Huerta, A., and Bowser, S. S.: Population Dynamics and Parasite Load of a Foraminifer on Its Antarctic Scallop Host with Their Carbonate Biomass Contributions, PLOS ONE, 10, e0132534, https://doi.org/10.1371/journal.pone.0132534, 2015.

Holland, K., Eggins, S. M., Hönisch, B., Haynes, L. L., and Branson, O.: Calcification rate and shell chemistry response of the planktic foraminifer Orbulina universa to changes in microenvironment seawater carbonate chemistry, Earth and Planetary Science Letters, 464, 124–134, https://doi.org/10.1016/j.epsl.2017.02.018, 2017.

Hönisch, B., Allen, K. A., Russell, A. D., Eggins, S. M., Bijma, J., Spero, H. J., Lea, D. W., and Yu, J.: Planktic foraminifers as recorders of seawater Ba/Ca, Marine Micropaleontology, 79, 52–57, https://doi.org/10.1016/j.marmicro.2011.01.003, 2011.

Horton, T., Kroh, A., Ahyong, S., Bailly, N., Boyko, C. B., Brandão, S. N., Gofas, S., Hooper, J. N. A., Hernandez, F., Holovachov, O., Mees, J., Molodtsova, T. N., Paulay, G., Decock, W., Dekeyzer, S., Poffyn, G., Vandepitte, L., Vanhoorne, B., Adlard, R., Agatha, S., Ahn, K. J., Akkari, N., Alvarez, B., Anderberg, A., Anderson, G., Angel, M. v, Antic, D., Arango, C., Artois, T., Atkinson, S., Auffenberg, K., Baldwin, B. G., Bank, R., Barber, A., Barbosa, J. P., Bartsch, I., Bellan-Santini, D., Bergh, N., Bernot, J., Berta, A., Bezerra, T. N., Bieler, R., Blanco, S., Blasco-Costa, I., Blazewicz, M., Bock, P., Bonifacino de León, M., Böttger-Schnack, R., Bouchet, P., Boury-Esnault, N., Boxshall, G., Bray, R., Bruce, N. L., Cairns, S., Calvo Casas, J., Carballo, J. L., Cárdenas, P., Carstens, E., Chan, B. K., Chan, T. Y., Cheng, L., Christenhusz, M., Churchill, M., Coleman, C. O., Collins, A. G., Collins, G. E., Corbari, L., Cordeiro, R., Cornils, A., Coste, M., Costello, M. J., Crandall, K. A., Cremonte, F., Cribb, T., Cutmore, S., Dahdouh-Guebas, F., Daly, M., Daneliya, M., Dauvin, J. C., Davie, P., de Broyer, C., de Grave, S., de Mazancourt, V., de Voogd, N. J., Decker, P., Defaye, D., d'Hondt, J. L., Dippenaar, S., Dohrmann, M., Dolan, J., Domning, D., Downey, R., Ector, L., Eisendle-Flöckner, U., Eitel, M., Encarnação, S. C. d., Enghoff, H., Epler, J., Ewers-Saucedo, C., et al.: World Register of Marine Species (WoRMS), http://www.marinespecies.org, 2021.

Immenhauser, A., Schöne, B. R., Hoffmann, R., and Niedermayr, A.: Mollusc and brachiopod skeletal hard parts: Intricate archives of their marine environment, Sedimentology, 63, 1–59, https://doi.org/10.1111/sed.12231, 2016.

Jacob, D. E., Wirth, R., Soldati, A. L., Wehrmeister, U., and Schreiber, A.: Amorphous calcium carbonate in the shells of adult Unionoida, Journal of Structural Biology, 173, 241–249, https://doi.org/10.1016/j.jsb.2010.09.011, 2011.

Jacob, D. E., Wirth, R., Agbaje, O. B. A., Branson, O., and Eggins, S. M.: Planktic foraminifera form their shells via metastable carbonate phases, Nature Communications, 8, 1–8, https://doi.org/10.1038/s41467-017-00955-0, 2017.

Jacobson, P.: Physical Oceanography of the Trondheimsfjord, Geophysical & Astrophysical Fluid Dynamics, 26, 3–26, https://doi.org/10.1080/03091928308221761, 1983.

Jochum, K. P., Nohl, U., Herwig, K., Lammel, E., Stoll, B., and Hofmann, A. W.: GeoReM: A New Geochemical Database for Reference Materials and Isotopic Standards, Geostandards and Geoanalytical Research, 29, 333–338, https://doi.org/10.1111/j.1751-908X.2005.tb00904.x, 2005.

Kato, K., Wada, H., and Fujioka, K.: The application of chemical staining to separate calcite and aragonite minerals for micro-scale isotopic analyses, Geochemical Journal, 37, 291–297, https://doi.org/10.2343/geochemj.37.291, 2003.

Klein, R. T., Lohmann, K. C., and Thayer, C. W.: Sr/Ca and 13C/12C ratios in skeletal calcite of Mytilus trossulus: Covariation with metabolic rate, salinity, and carbon isotopic composition of seawater, Geochimica et Cosmochimica Acta, https://doi.org/10.1016/S0016-7037(96)00232-3, 1996.

Koho, K. A., de Nooijer, L. J., and Reichart, G. J.: Combining benthic foraminiferal ecology and shell Mn/Ca to deconvolve past bottom water oxygenation and paleoproductivity, Geochimica et Cosmochimica Acta, 165, 294–306, https://doi.org/10.1016/j.gca.2015.06.003, 2015.

Lantz, B.: The impact of sample non-normality on ANOVA and alternative methods, British Journal of Mathematical and Statistical Psychology, 66, 224–244, https://doi.org/10.1111/j.2044-8317.2012.02047.x, 2013.

Lear, C. H. and Rosenthal, Y.: Benthic foraminiferal Li/Ca: Insights into Cenozoic seawater carbonate saturation state, Geology, 34, 985, https://doi.org/10.1130/G22792A.1, 2006.

Lear, C. H., Rosenthal, Y., and Slowey, N.: Benthic foraminiferal Mg/Ca-paleothermometry: A revised core-top calibration, Geochimica et Cosmochimica Acta, 66, 3375–3387, https://doi.org/10.1016/S0016-7037(02)00941-9, 2002.

949 Lorens, R. B.: Sr, Cd, Mn and Co distribution coefficients in calcite as a function of calcite precipitation
950 rate, Geochimica et Cosmochimica Acta, 45, 553–561, https://doi.org/10.1016/0016-7037(81)90188-
951 5, 1981.

952 Lorens, R. B. and Bender, M. L.: The impact of solution chemistry on *Mytilus edulis* calcite and
953 aragonite, Geochimica et Cosmochimica Acta, 44, 1265–1278, https://doi.org/10.1016/0016-
954 7037(80)90087-3, 1980.

955 Lorrain, A., Gillikin, D. P., Paulet, Y. M., Chauvaud, L., le Mercier, A., Navez, J., and André, L.: Strong
956 kinetic effects on Sr/Ca ratios in the calcitic bivalve Pecten maximus, Geology, 33, 965–968,
957 https://doi.org/10.1130/G22048.1, 2005.

958 Mackensen, A. and Nam, S. il: Taxon-specific epibenthic foraminiferal δ18O in the Arctic Ocean:
959 Relationship to water masses, deep circulation, and brine release, Marine Micropaleontology, 113,
960 34–43, https://doi.org/10.1016/j.marmicro.2014.09.002, 2014.

961 Marchitto, T. M., Curry, W. B., Lynch-Stieglitz, J., Bryan, S. P., Cobb, K. M., and Lund, D. C.: Improved
962 oxygen isotope temperature calibrations for cosmopolitan benthic foraminifera, Geochimica et
963 Cosmochimica Acta, 130, 1–11, https://doi.org/10.1016/j.gca.2013.12.034, 2014.

964 Marin, F., Luquet, G., Marie, B., and Medakovic, D.: Molluscan Shell Proteins: Primary Structure,
965 Origin, and Evolution, Current Topics in Developmental Biology, 80, 209–276,
966 https://doi.org/10.1016/S0070-2153(07)80006-8, 2007.

967 McConnaughey, T. A.: Sub-equilibrium oxygen-18 and carbon-13 levels in biological carbonates:
968 Carbonate and kinetic models, Coral Reefs, 22, 316–327, https://doi.org/10.1007/s00338-003-0325-
969 2, 2003.

970 McCorkle, D. C., Corliss, B. H., and Farnham, C. A.: Vertical distributions and stable isotopic
971 compositions of live (stained) benthic foraminifera from the North Carolina and California continental
972 margins, Deep-Sea Research Part I: Oceanographic Research Papers, 44, 983–1024,
973 https://doi.org/10.1016/S0967-0637(97)00004-6, 1997.

974 McCulloch, M., Falter, J., Trotter, J., and Montagna, P.: Coral resilience to ocean acidification and
975 global warming through pH up-regulation, Nature Climate Change, 2, 623–627,
976 https://doi.org/10.1038/nclimate1473, 2012.

977 Mienis, F., de Stigter, H. C., White, M., Duineveld, G., de Haas, H., and van Weering, T. C. E.:
978 Hydrodynamic controls on cold-water coral growth and carbonate-mound development at the SW

and SE Rockall Trough Margin, NE Atlantic Ocean, Deep-Sea Research Part I: Oceanographic Research Papers, 54, 1655–1674, https://doi.org/10.1016/j.dsr.2007.05.013, 2007.

Milzer, G., Giraudeau, J., Faust, J., Knies, J., Eynaud, F., and Rühlemann, C.: Spatial distribution of benthic foraminiferal stable isotopes and dinocyst assemblages in surface sediments of the Trondheimsfjord, central Norway, Biogeosciences, 10, 4433–4448, https://doi.org/10.5194/bg-10-4433-2013, 2013.

Moradian-Oldak, J., Addadi, L., Weiner, S., and Berman, A.: Tuning of Crystal Nucleation and Growth by Proteins: Molecular Interactions at Solid-Liquid Interfaces in Biomineralization, Croatica Chemica Acta, 63, 539–544, 1990.

Mucci, A.: Manganese uptake during calcite precipitation from seawater: Conditions leading to the formation of a pseudokutnahorite, Geochimica et Cosmochimica Acta, 52, 1859–1868, https://doi.org/10.1016/0016-7037(88)90009-9, 1988.

Mucci, A. and Morse, J. W.: The incorporation of Mg 2+ and Sr 2+ into calcite overgrowths: influences of growth rate and solution composition, Geochimica et Cosmochimica Acta, 47, 217–233, 1983.

Nakahara, H.: Nacre Formation in Bivalve and Gastropod Molluscs, in: Mechanisms and Phylogeny of Mineralization in Biological Systems, Springer Japan, Tokyo, 343–350, https://doi.org/10.1007/978-4-431-68132-8_55, 1991.

Nehrke, G., Keul, N., Langer, G., de Nooijer, L. J., Bijma, J., and Meibom, A.: A new model for biomineralization and trace-element signatures of Foraminifera tests, Biogeosciences, https://doi.org/10.5194/bg-10-6759-2013, 2013.

de Nooijer, L. J., Toyofuku, T., and Kitazato, H.: Foraminifera promote calcification by elevating their intracellular pH, Proceedings of the National Academy of Sciences of the United States of America, 106, 15374–15378, https://doi.org/10.1073/pnas.0904306106, 2009.

de Nooijer, L. J., Spero, H. J., Erez, J., Bijma, J., and Reichart, G. J.: Biomineralization in perforate foraminifera, Earth-Science Reviews, 135, 48–58, https://doi.org/10.1016/j.earscirev.2014.03.013, 2014.

Oomori, T., Kaneshima, H., Maezato, Y., and Kitano, Y.: Distribution Coefficient of Mg2+ ions between calcite and solution at 10-50°C, Marine Chemistry, 20, 327–336, https://doi.org/10.1016/B978-044452228-3/50006-6, 1987.

1008 Petersen, J., Barras, C., Bézos, A., La, C., de Nooijer, L. J., Meysman, F. J. R., Mouret, A., Slomp, C. P.,
1009 and Jorissen, F. J.: Mn/Ca intra- and inter-test variability in the benthic foraminifer Ammonia tepida,
1010 Biogeosciences, 15, 331–348, https://doi.org/10.5194/bg-15-331-2018, 2018.

1011 Piez, K. A.: Amino Acid Composition of Some Calcified Proteins, Science, 134, 841–842,
1012 https://doi.org/10.1126/science.134.3482.841, 1961.

1013 Pytkowicz, R. M.: Rates of Inorganic Calcium Carbonate Nucleation, The Journal of Geology, 73, 196–
1014 199, https://doi.org/10.1086/627056, 1965.

1015 Raddatz, J., Rüggeberg, A., Margreth, S., and Dullo, W. C.: Paleoenvironmental reconstruction of
1016 Challenger Mound initiation in the Porcupine Seabight, NE Atlantic, Marine Geology, 282, 79–90,
1017 https://doi.org/10.1016/j.margeo.2010.10.019, 2011.

1018 Raddatz, J., Liebetrau, V., Rüggeberg, A., Hathorne, E., Krabbenhöft, A., Eisenhauer, A., Böhm, F.,
1019 Vollstaedt, H., Fietzke, J., López Correa, M., Freiwald, A., and Dullo, W. C.: Stable Sr-isotope, Sr/Ca,
1020 Mg/Ca, Li/Ca and Mg/Li ratios in the scleractinian cold-water coral *Lophelia pertusa*, Chemical
1021 Geology, 352, 143–152, https://doi.org/10.1016/j.chemgeo.2013.06.013, 2013.

1022 Raddatz, J., Rüggeberg, A., Flögel, S., Hathorne, E. C., Liebetrau, V., Eisenhauer, A., and Dullo, W. C.:
1023 The influence of seawater pH on U/Ca ratios in the scleractinian cold-water coral Lophelia pertusa,
1024 Biogeosciences, 11, 1863–1871, https://doi.org/10.5194/bg-11-1863-2014, 2014.

1025 Raddatz, J., Nürnberg, D., Tiedemann, R., and Rippert, N.: Southeastern marginal West Pacific Warm
1026 Pool sea-surface and thermocline dynamics during the Pleistocene (2.5–0.5 Ma), Palaeogeography,
1027 Palaeoclimatology, Palaeoecology, 471, 144–156, https://doi.org/10.1016/j.palaeo.2017.01.024,
1028 2017.

1029 Raitzsch, M., Duenas-Bohórquez, A., Reichart, G. J., de Nooijer, L. J., and Bickert, T. T.: Incorporation
1030 of Mg and Sr in calcite of cultured benthic foraminifera: Impact of calcium concentration and
1031 associated calcite saturation state, Biogeosciences, 7, 869–881, https://doi.org/10.5194/bg-7-869-
1032 2010, 2010.

1033 Raja, R., Saraswati, P. K., Rogers, K., and Iwao, K.: Magnesium and strontium compositions of recent
1034 symbiont-bearing benthic foraminifera, Marine Micropaleontology, 58, 31–44,
1035 https://doi.org/10.1016/j.marmicro.2005.08.001, 2005.

1036 Rathburn, A. E. and de Deckker, P.: Magnesium and strontium compositions of Recent benthic
1037 foraminifera from the Coral Sea, Australia and Prydz Bay, Antarctica, Marine Micropaleontology, 32,
1038 231–248, https://doi.org/10.1016/S0377-8398(97)00028-5, 1997.

1039 Schleinkofer, N., Raddatz, J., Freiwald, A., Evans, D., Beuck, L., Rüggeberg, A., and Liebetrau, V.:
1040 Environmental and biological controls on Na/Ca ratios in scleractinian cold-water corals,
1041 Biogeosciences, 16, 3565–3582, https://doi.org/10.5194/bg-16-3565-2019, 2019.

1042 Schleinkofer, N., Raddatz, J., Evans, D., Gerdes, A., Flögel, S., Voigt, S., Büscher, J. V., and Wisshak, M.:
1043 Compositional variability of Mg/Ca, Sr/Ca, and Na/Ca in the deep-sea bivalve Acesta excavata
1044 (Fabricius, 1779), PLOS ONE, 16, e0245605, https://doi.org/10.1371/journal.pone.0245605, 2021.

1045 Schöne, B. R., Zhang, Z., Jacob, D., Gillikin, D. P., Tütken, T., Garbe-Schönberg, D., McConnaughey, T.,
1046 and Soldati, A.: Effect of organic matrices on the determination of the trace element chemistry (Mg,
1047 Sr, Mg/Ca, Sr/Ca) of aragonitic bivalve shells (*Arctica islandica*) - Comparison of ICP-OES and LA-ICP-
1048 MS data, Geochemical Journal, 44, 23–37, https://doi.org/10.2343/geochemj.1.0045, 2010.

1049 Schweizer, M., Bowser, S. S., Korsun, S., and Pawlowski, J.: Emendation of Cibicides antarcticus
1050 (Saidova, 1975) based on molecular, morphological, and ecological data, Journal of Foraminiferal
1051 Research, https://doi.org/10.2113/gsjfr.42.4.340, 2012.

1052 Secor, C. L., Mills, E. L., Harshbarger, J., Kuntz, H. T., Gutenmann, W. H., and Lisk, D. J.:
1053 Bioaccumulation of toxicants, element and nutrient composition, and soft tissue histology of zebra
1054 mussels (Dreissena polymorpha) from New York State waters, Chemosphere,
1055 https://doi.org/10.1016/0045-6535(93)90224-S, 1993.

1056 Segev, E. and Erez, J.: Effect of Mg/Ca ratio in seawater on shell composition in shallow benthic
1057 foraminifera, Geochemistry, Geophysics, Geosystems, 7, 1–8,
1058 https://doi.org/10.1029/2005GC000969, 2006.

1059 Smith, P. B. and Emiliani, C.: Oxygen-isotope analysis of recent tropical pacific benthonic
1060 foraminifera, Science, https://doi.org/10.1126/science.160.3834.1335, 1968.

1061 Spero, H. J.: Ultrastructural examination of chamber morphogenesis and biomineralization in the
1062 planktonic foraminifer Orbulina universa, Marine Biology, 99, 9–20,
1063 https://doi.org/10.1007/BF00644972, 1988.

1064 Spötl, C. and Vennemann, T. W.: Continuous-flow isotope ratio mass spectrometric analysis of
1065 carbonate minerals, Rapid Communications in Mass Spectrometry, 17, 1004–1006,
1066 https://doi.org/10.1002/rcm.1010, 2003.

1067 Stephenson, A. E., Deyoreo, J. J., Wu, L., Wu, K. J., Hoyer, J., and Dove, P. M.: Peptides enhance
1068 magnesium signature in calcite: Insights into origins of vital effects, Science, 322, 724–727,
1069 https://doi.org/10.1126/science.1159417, 2008.

1070 Sunda, W. G. and Huntsman, S. A.: Regulation of cellular manganese and manganese transport rates
1071 in the unicellular alga Chlamydomonas, Limnology and Oceanography, 30, 71–80,
1072 https://doi.org/10.4319/lo.1985.30.1.0071, 1985.

1073 Swinehart, J. H. and Smith, K. W.: Iron And Manganese Deposition In The Periostraca Of Several
1074 Bivalve Molluscs, The Biological Bulletin, 156, 369–381, https://doi.org/10.2307/1540924, 1979.

1075 Takesue, R. K., Bacon, C. R., and Thompson, J. K.: Influences of organic matter and calcification rate
1076 on trace elements in aragonitic estuarine bivalve shells, Geochimica et Cosmochimica Acta, 72, 5431–
1077 5445, https://doi.org/10.1016/j.gca.2008.09.003, 2008.

1078 Tambutté, E., Allemand, D., Zoccola, D., Meibom, A., Lotto, S., Caminiti, N., and Tambutté, S.:
1079 Observations of the tissue-skeleton interface in the scleractinian coral Stylophora pistillata, Coral
1080 Reefs, 26, 517–529, https://doi.org/10.1007/s00338-007-0263-5, 2007.

1081 Todd, R.: A new Rosalina (foraminifera) parasitic on a bivalve, Deep-Sea Research and Oceanographic
1082 Abstracts, 12, 831–837, https://doi.org/10.1016/0011-7471(65)90806-5, 1965.

1083 Toyofuku, T., Kitazato, H., Kawahata, H., Tsuchiya, M., and Nohara, M.: Evaluation of Mg/Ca
1084 thermometry in foraminifera: Comparison of experimental results and measurements in nature,
1085 Paleoceanography, 15, 456–464, https://doi.org/10.1029/1999PA000460, 2000.

1086 Toyofuku, T., Matsuo, M. Y., de Nooijer, L. J., Nagai, Y., Kawada, S., Fujita, K., Reichart, G. J., Nomaki,
1087 H., Tsuchiya, M., Sakaguchi, H., and Kitazato, H.: Proton pumping accompanies calcification in
1088 foraminifera, Nature Communications, 8, 1–6, https://doi.org/10.1038/ncomms14145, 2017.

1089 Tribovillard, N., Algeo, T. J., Lyons, T., and Riboulleau, A.: Trace metals as paleoredox and
1090 paleoproductivity proxies: An update, Chemical Geology, 232, 12–32,
1091 https://doi.org/10.1016/j.chemgeo.2006.02.012, 2006.

1092 Vénec-Peyré, M. T.: Bioeroding foraminifera: A review, Marine Micropaleontology, 28, 19–30,
1093 https://doi.org/10.1016/0377-8398(95)00037-2, 1996.

1094 de Villiers, S., Nelson, B. K., and Chivas, A.: Biological Control on Coral Sr/Ca and d18O
1095 Reconstructions of Sea Surface Temperatures, Science, 269, 1247–1249, 1995.

1096 Wada, K. and Fujinuki, T.: Biomineralization in bivalve molluscs with emphasis on the chemical
1097 composition of the extrapallial flui, Book chapter, 1976.

1098 Walker, S. E., Hancock, L. G., and Bowser, S. S.: Diversity, biogeography, body size and fossil record of
1099 parasitic and suspected parasitic foraminifera: A review, Journal of Foraminiferal Research, 47, 34–
1100 55, https://doi.org/10.2113/gsjfr.47.1.34, 2017.

Webb, A. E., Pomponi, S. A., van Duyl, F. C., Reichart, G. J., and de Nooijer, L. J.: pH Regulation and Tissue Coordination Pathways Promote Calcium Carbonate Bioerosion by Excavating Sponges, Scientific Reports, 9, 1–10, https://doi.org/10.1038/s41598-018-36702-8, 2019.

Whitney, N. M., Johnson, B. J., Dostie, P. T., Luzier, K., and Wanamaker, A. D.: Paired bulk organic and individual amino acid δ15N analyses of bivalve shell periostracum: A paleoceanographic proxy for water source variability and nitrogen cycling processes, Geochimica et Cosmochimica Acta, 254, 67–85, https://doi.org/10.1016/j.gca.2019.03.019, 2019.

Wilbur, K. M. and Saleuddin, A. S. M.: Shell Formation, in: The Mollusca, Elsevier, 235–287, https://doi.org/10.1016/B978-0-12-751404-8.50014-1, 1983.

Yin, Y., Huang, J., Paine, M. L., Reinhold, V. N., and Chasteen, N. D.: Structural Characterization of the Major Extrapallial Fluid Protein of the Mollusc Mytilus edulis : Implications for Function, Biochemistry, 44, 10720–10731, https://doi.org/10.1021/bi0505565, 2005.

Yu, X. and Inesi, G.: Variable stoichiometric efficiency of Ca2+ and Sr2+ transport by the sarcoplasmic reticulum ATPase, Journal of Biological Chemistry, 270, 4361–4367, https://doi.org/10.1074/jbc.270.9.4361, 1995.

Zhang, C. and Zhang, R.: Matrix proteins in the outer shells of molluscs, Marine Biotechnology, 8, 572–586, https://doi.org/10.1007/s10126-005-6029-6, 2006.